Microwave quantum optics and electron transport through a metallic dot strongly coupled to a transmission line cavity

Bergenfeldt, Christian; Samuelsson, Peter

Published in:
Physical Review B (Condensed Matter and Materials Physics)

DOI:
10.1103/PhysRevB.85.045446

2012

Microwave quantum optics and electron transport through a metallic dot strongly coupled to a transmission line cavity

C. Bergenfeldt and P. Samuelsson
Division of Mathematical Physics, Lund University, Box 118, SE-221 00 Lund, Sweden
(Received 31 October 2011; published 31 January 2012)

We investigate theoretically the properties of the photon state and the electronic transport in a system consisting of a metallic quantum dot strongly coupled to a superconducting microwave transmission line cavity. Within the framework of circuit quantum electrodynamics, we derive a Hamiltonian for arbitrary strong capacitive coupling between the dot and the cavity. The dynamics of the system is described by a quantum master equation, accounting for the electronic transport as well as the coherent, nonequilibrium properties of the photon state. The photon state is investigated, focusing on, for a single active mode, signatures of microwave polaron formation and the effects of a nonequilibrium photon distribution. For two active photon modes, the intermode conversion and polaron coherences are investigated. For the electronic transport, electrical current and noise through the dot and the influence of the photon state on the transport properties are at the focus. We identify clear transport signatures due to the nonequilibrium photon population, in particular the emergence of superpoissonian shot noise at ultrastrong dot-cavity couplings.

DOI: 10.1103/PhysRevB.85.045446 PACS number(s): 73.23.Hk, 72.10.Di, 85.25.−j

I. INTRODUCTION

The field of circuit quantum electrodynamics (QED) has over the last decade emerged as an on-chip version of cavity QED. In circuit QED, the interaction between solid-state quantum systems and high-quality on-chip circuit elements is investigated. The pioneering works of the Yale group proposed[1] and demonstrated[2] strong coupling between a superconducting qubit and a microwave transmission line resonator. This opened up for an impressive development in the field of quantum information processing with superconducting circuits,[3] with a number of key experiments demonstrating long distance qubit state transfer,[4,5] controllable multiqubit entanglement,[6] and the execution of basic quantum algorithms.[7] Recently also nanoscale qubits, based on semiconductor nanowires or carbon nanotubes, coupled to transmission lines, have received increasing attention.[8–14] A parallel development is considering the possibilities to perform fundamental quantum optics experiments with microwave photons in cavities. Experiments on microwave quantum optics range from arbitrary photon state preparation[15] and entanglement of cavity photons[16] to single photon generation,[17] microwave lasing[18] and fast tuning of cavity photon properties.[19,20]

An important recent development is the effort to reach the ultrastrong coupling regime, where the strength of the coupling between the qubit and the cavity becomes comparable to the frequency of the fundamental cavity mode. In this regime, the Jaynes-Cummings model breaks down and new physical effects become important. Recent experiments[21–23] with flux qubits directly coupled to a superconductor transmission line cavity demonstrated couplings of the order of ten percent of the resonator frequency. These findings spurred a number of theoretical works on microwave quantum optics in the ultrastrong regime, see, e.g., Refs. 24–26.

Lately, also systems with mesoscopic or nanoscale conductors, such as Josephson junctions,[27–29] superconducting single-electron transistors[18,28,30] and quantum dots,[31–34] inserted into microwave cavities have been investigated. In particular, the spectral properties of microwaves emitted from a Josephson junction in the dynamical Coulomb blockade regime were investigated in Ref. 29. Also, in a number of very recent experiments, single[31,32] and double[33] quantum dots were coupled to external leads and the electronic transport was investigated via the scattering properties of injected microwaves. Moreover, microwave lasing with population inversion caused by electron tunneling through a superconducting single-electron transistor was demonstrated experimentally[18] and investigated theoretically.[30,35] These experimental achievements open up for a detailed investigation of the interplay of transport electrons and individual cavity photons. Of particular interest is the *strong-coupling* regime, where the rate for tunnel-induced photon excitation (and deexcitation) is much larger than the intrinsic cavity photon decay rate. In this regime, the photon distribution is nonequilibrium and back action of the tunnel-induced photons on the transported electrons becomes important. This will introduce new physical effects, beyond what was investigated in earlier works where electronic transport through conductors in the presence of a thermalized electromagnetic environment was at the focus.[27–29,36–41]

The *ultrastrong-coupling* regime in transport corresponds to a coupling strength between the transport electrons and cavity photons of the order of the frequency of the fundamental mode of the cavity. In this regime, electrons entering the conductor strongly modify the photon states of the cavity and microwave polarons are formed. To the best of our knowledge, the ultrastrong coupling regime has not been reached experimentally in conductor-cavity systems. In this context, it is interesting to point out the strong similarities between the physics of transport through conductors coupled to microwave cavities and molecular electronics and nanoelectromechanics, where the conduction electrons couple to vibrational degrees of freedom, or phonons.[42–47] In fact, in these type of systems, ultrastrong electron-phonon coupling has recently been demonstrated.[46,47] Several nontrivial transport properties resulting from a nonequilibrium phonon distribution has further been investigated theoretically in this regime, e.g., super-Poissonian[48] or suppressed[49] shot noise and negative differential conductance.[43,50–52] Moreover, the nonequilibrium

phonon distribution itself has been found to possess nontrivial properties.[51,53–56] These results clearly promote investigations of electron-photon analogs of electron-phonon phenomena, performed in strongly-coupled conductor-cavity systems.

Taken together, these observations provide strong motivation for a careful theoretical investigation of the regimes of strong and ultrastrong couplings between electrical conductors and microwave cavities. In this work, we present a detailed investigation of a conductor capacitively coupled to a microwave cavity, focusing on the properties of the electronic transport through the conductor and the transport-induced photon state in the cavity. The conductor is taken to be an electrostatically gated metallic dot, a single-electron transistor, in the normal state. The combined all-metal dot-cavity system can be realized with existing lithographic techniques, giving large experimental versatility when trying to increase the coupling strength. Moreover, as we demonstrate in this work, the metallic dot-cavity system allows for a detailed and consistent strong-coupling analysis, analytical as well as numerical, of the deep quantum, few-photon regime where interesting, new physical phenomena are most clearly manifested. We point out that albeit focusing on a metallic dot conductor, our approach can directly be applied to few-level quantum dots.

In the first part of the paper, we provide a detailed description of the dot-cavity system and describe how to derive, based on the Lagrangian formulation of circuit QED, a Hamiltonian for the isolated dot-cavity system for arbitrary strong coupling. We demonstrate the importance of a consistent strong-coupling treatment in order to avoid unphysical effects that would follow from a naive extension of the weak-coupling model to stronger couplings. We also discuss possible experimental realizations of the strong capacitive-coupling regime relevant for our model. For the dot coupled to external leads, the total system is described by a quantum master equation that accounts for both the electronic transport in the sequential tunneling regime as well as the coherent, nonequilibrium dynamics of the photon state. We first analyze the properties of the photon state for the cases where one and two photon modes in the cavity are active. For a single active mode, we describe the transport-induced photon state for different dot-cavity couplings, focusing on the nonequilibrium distribution and the signatures of microwave polaron formation. Analytical results are obtained in the limit where the coupling strength is small compared to the fundamental frequency of the cavity. For two active modes, we investigate the intermode conversion of photons and, in particular, the coherence properties of the photon state, important in the ultrastrong coupling regime. An effective model for the maximally coherent situation is presented, allowing us to find accurate expressions for the photon state also at ultrastrong couplings. Turning to the electron transport, the conductance and the noise through the dot is analyzed for different dot-cavity coupling strengths. For coupling strengths much smaller than the fundamental frequency of the cavity, the current and noise are shown to be independent on the photon state. For stronger couplings, the current and noise are compared to results for an equilibrated photon state and we identify clear effects on the transport due to the nonequilibrium photon state. Most prominently, we find super-Poissonian noise at ultrastrong couplings, an indication of the avalanche effect discussed for molecular electronics in Ref. 48.

II. SYSTEM AND METHOD

We consider the system shown in Fig. 1. A normal-state metallic dot is inserted between the central conductor and one of the ground planes in a superconducting transmission line cavity. The cavity has a length d and the dot is placed a distance a from the left end. C and C_D denotes the capacitance between the dot and ground and between the dot and the cavity central conductor, respectively. The cavity has a characteristic impedance $Z_0 = \sqrt{L_0/C_0}$, where L_0 and C_0 are the inductance and capacitance per unit length, respectively. The central conductor can be made of a superconducting material or a metamaterial, e.g., a superconducting quantum interference device (SQUID) array.[57,58] The dot is further tunnel coupled to electronic leads $\ell = L, R$, kept at bias voltages V_ℓ. We assume that the lead-dot resistances are much larger than the quantum resistance quantum $R_q = h/e^2$; the transport is in the Coulomb blockade regime with a well defined charge on the dot. The background charge on the dot can be controlled with a gate electrode, kept at a bias V_g, via a gate capacitance denoted C_g.

The leads are assumed to be in thermal equilibrium at temperature T. Concerning the internal dynamics of the dot, electron-electron and electron-phonon scattering rates are much larger than the electron tunneling rate. As a consequence, the dot electrons reach thermal equilibrium, at the temperature T, in between each tunneling event. Moreover, collective internal excitations of the dot, i.e., plasmons, which have energies in the ultraviolet range, much larger than the other relevant energy-scales of the problem, are not considered.

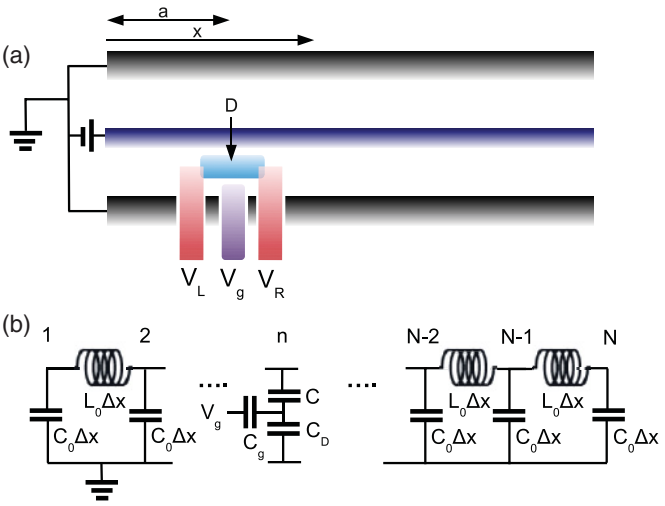

FIG. 1. (Color online) (a) Schematic of the system with a normal-state metallic dot (D) inserted in a transmission line cavity a distance a from the left end. The central conductor (blue) can be a superconductor or an array of SQUIDs. The dot is tunnel coupled to two metallic leads L and R (red) kept at voltages V_L and V_R, respectively. The dot is capacitively coupled to a gate electrode (purple) kept at the voltage V_g. (b) Discrete circuit representation of the dot-cavity system with N nodes. The dot is connected to node n. The inductance between two adjacent nodes is $L_0\Delta x$ and the capacitance to ground from node $i \neq n$ is $C_0\Delta x$, giving the cavity a characteristic impedance $\sqrt{L_0/C_0}$. The dot-cavity capacitance is C, the dot-to-ground capacitances is C_D, and the gate capacitance is C_g.

The relaxation of the photons in the cavity due to electron tunneling is much faster than the the intrinsic relaxation rate κ in high-quality cavities, and we thus neglect all intrinsic sources of photon loss.

A. Cavity-dot system

Our initial aim is to arrive at a Hamiltonian for the total system, without any approximation on the dot-cavity coupling strength. We start by considering the isolated dot-cavity system and derive a Hamiltonian expressed in terms of the charge on the dot, the photons in the cavity and the interaction between them. Following standard circuit QED procedure,[59,60] we first write down the Lagrangian for the circuit. We note that similar systems, with the focus on arbitrary strong dot-cavity coupling, have been treated in Refs. 61 and 62. The discussion here is therefore kept short and details are presented only where our derivation differs from previous works.

The transmission line cavity is represented by a chain of $N \gg 1$ identical LC circuits with capacitance $C_0\Delta x$ and inductance $L_0\Delta x$, where $\Delta x = d/N$. The quantum dot is coupled to the chain node $n = Na/d$ and to ground via capacitances C and C_D, respectively. The Lagrangian of the circuit is then

$$L = \sum_{i\neq n}^{N} \frac{C_0\Delta x\dot{\phi}_i^2}{2} - \sum_{i}^{N-1} \frac{(\phi_{i+1}-\phi_i)^2}{2L_0\Delta x} + \frac{C_D\dot{\phi}_D^2}{2} + \frac{C(\dot{\phi}_n-\dot{\phi}_D)^2}{2} + \frac{C_g(V_g+\dot{\phi}_D)^2}{2}, \quad (1)$$

where ϕ_i is the phase of the ith node and ϕ_D the phase of the dot.

To find the normal modes[63] of the combined cavity-dot system, we consider the Euler-Lagrange equations $\frac{d}{dt}\frac{\partial L}{\partial\dot{\phi}_i} - \frac{\partial L}{\partial\phi_i} = 0$, for $i = 1,\ldots,N,D$. Using the equation for $i = D$, $\ddot{\phi}_D$ can be expressed in terms of $\ddot{\phi}_N$ and substituted into the equation for $i = N$. We can then write the equations for the cavity phases in matrix form:

$$\mathcal{T}\ddot{\boldsymbol{\phi}} = \mathcal{V}\boldsymbol{\phi}, \quad (2)$$

where $\boldsymbol{\phi} = [\phi_1,\ldots,\phi_N]^T$ and the matrices $\mathcal{T}$ and $\mathcal{V}$ have elements $\mathcal{T}_{ij} = \delta_{ij}[C_0\Delta x + \frac{C(C_0\Delta x+C_g)}{C+C_D+C_g}\delta_{in}]$ and $\mathcal{V}_{ij} = \frac{1}{L_0\Delta x}[\delta_{ij}(2-\delta_{i1}-\delta_{iN}) - \delta_{i(j-1)} - \delta_{i(j+1)}]$. Since $\mathcal{T}$ is diagonal with positive elements and $\mathcal{V}$ is real and symmetric, we can express Eq. (2) in the basis of normal modes as $\ddot{\boldsymbol{\varphi}} = \Lambda\boldsymbol{\varphi}$, where $\boldsymbol{\phi} = M\boldsymbol{\varphi}$. The elements Λ_p of the diagonal matrix Λ are the frequencies of the normal modes squared, i.e., $\Lambda_p = \omega_p^2$. The columns, $\mathbf{m}_p$, in M are the solutions to the eigenvalue problem

$$\mathcal{T}^{-1}\mathcal{V}\mathbf{m}_p = \omega_p^2\mathbf{m}_p, \quad (3)$$

with the normalization condition $\mathbf{m}_p^T\mathcal{T}\mathbf{m}_q = C_0d\delta_{pq}$. We can then express the Lagrangian in terms of the normal modes as

$$L = \sum_p\left(\frac{C_0d\dot{\varphi}_p^2}{2} - \frac{C_0d\omega_p^2\varphi_p^2}{2}\right) + \frac{C^2}{2C_\Sigma}\sum_{pq}M_{np}M_{nq}\dot{\varphi}_p\dot{\varphi}_q + C_gV_g\dot{\varphi}_D + \frac{C_D\dot{\varphi}_D^2}{2} - C\dot{\varphi}_D\sum_p M_{np}\dot{\varphi}_p, \quad (4)$$

where $C_\Sigma = C_D + C + C_g$ and we write $\phi_D = \varphi_D$ for notational convenience.

In the continuum limit, $N\to\infty$, $\Delta x\to 0$ with $N\Delta x = d$ constant, the vectors $\mathbf{m_p}$ turn into continuous functions $\zeta_p(x)$ of the coordinate x along the transmission line. From Eq. (3), it is found that the functions $\zeta_p(x)$ satisfy the differential equation

$$\zeta_p''(x) + k_p^2[1 + d\alpha\delta(x-a)]\zeta_p(x) = 0, \quad (5)$$

with boundary conditions $\zeta_p'(0) = \zeta_p'(d) = 0$. Here, $k_p = \sqrt{L_0C_0}\omega_p$ and $\alpha = C_gC/(C_\Sigma C_0d)$. The normalization condition above becomes

$$\frac{1}{d}\int_0^d dx\zeta_p(x)\zeta_q(x)[1+\alpha d\delta(x-a)] = \delta_{pq}. \quad (6)$$

This generalized Sturm-Liouville problem has solutions

$$\zeta_p(x) = \begin{cases} A_p\cos(k_px), & 0\leqslant x\leqslant a, \\ B_p\cos[k_p(d-x)], & a\leqslant x\leqslant d, \end{cases} \quad (7)$$

where $A_p\cos(k_pa) = B_p\cos[k_p(d-a)]$ and k_p are the positive solutions of the equation

$$\frac{\tan(k_pd)[1+\tan^2(k_pa)]}{1+\tan(k_pa)\tan(k_pd)} = -\alpha k_pd, \quad (8)$$

following from Eq. (5) with boundary conditions. The solutions are illustrated in Fig. 2. The normalization condition in Eq. (6) gives

$$A_p^2 = \frac{d}{2}\left[a + \frac{\sin(2k_pa)}{2k_p} + \cos^2(k_pa)F_p\right]^{-1} \quad (9)$$

with

$$F_p = \frac{(d-a)}{\cos^2[k_p(d-a)]} + \frac{\tan[k_p(d-a)]}{2k_p} + \alpha d. \quad (10)$$

We see that in the limit $\alpha k_pd \ll 1$, corresponding to low frequencies ω_p, the solutions k_p in Eq. (8) approach $p\pi/d$, the result for the cavity disconnected from the dot. In the opposite limit, $\alpha k_pd \gg 1$, the solutions approach $(p+1/2)\pi/a$

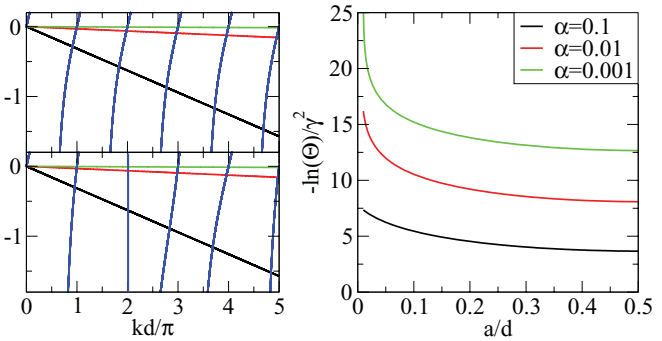

FIG. 2. (Color online) Left panels: intersections of the left- and right-hand sides of Eq. (8) for different α (see right panel inset). The ratios $a/d = 0$ and $a/d = 1/4$ for upper and lower panels, respectively. Right panel: position dependence of the renormalization factor $-\ln(\Theta)/\gamma^2$, with $\gamma = (C/C_\Sigma)\sqrt{Z_0/R_q}$. Only positions $0\leqslant a\leqslant d/2$ are plotted since the renormalization factor is symmetric with respect to $d/2$.

and $(p+1/2)\pi/(d-a)$. This gives, from Eq. (7) that the amplitudes $\zeta_p(x)$, at $x=a$, will be zero: for large ω_p, the cavity is effectively grounded via the dot.

Thus, in the continuum limit, we obtain the Lagrangian for the system:

$$L=\sum_p\left[\frac{C_C\dot{\varphi}_p^2}{2}-\frac{(k_pd)^2\varphi_p^2}{2L_C}\right]-C\dot{\varphi}_D\sum_p\zeta_p(a)\dot{\varphi}_p + \frac{C^2}{2C_\Sigma}\sum_{pq}\zeta_p(a)\zeta_q(a)\dot{\varphi}_p\dot{\varphi}_q+\frac{C_\Sigma\dot{\varphi}_D^2}{2}+C_gV_g\dot{\varphi}_D, \quad (11)$$

where $C_C=C_0d$ and $L_C=L_0d$ are the total capacitance and inductance of the cavity, respectively. This Lagrangian can now be used to obtain the conjugate variables $Q_D=\partial L/\partial\dot{\varphi}_D$ and $Q_p=\partial L/\partial\dot{\varphi}_p$ to φ_D and φ_p, respectively. We point out that Q_D is the charge on the dot.

Expressing $\dot{\varphi}_D$ and $\dot{\varphi}_p$ in terms of Q_D and Q_p and using the Legendre transformation, $H_S=Q_D\dot{\varphi}_D+\sum_pQ_p\dot{\varphi}_p-L$, the following classical Hamiltonian of the system is obtained:

$$H_S=\sum_p\left[\frac{Q_p^2}{2C_C}+\frac{(k_pd)^2\varphi_p^2}{2L_C}+\frac{C(Q_D-C_gV_g)}{C_\Sigma C_0}\zeta_p(a)Q_p\right] + \frac{(Q_D-C_gV_g)^2}{2C_\Sigma}\left[1+\frac{C^2}{C_\Sigma C_C}\sum_p\zeta_p(a)^2\right]. \quad (12)$$

The quantum Hamiltonian is obtained by canonical quantization. The generalized coordinates Q_p,φ_p,Q_D, and φ_D are replaced by operators $\hat{Q}_p,\hat{\varphi}_p,\hat{Q}_D$, and $\hat{\varphi}_D$ and the commutation relations $[\hat{Q}_p,\hat{\varphi}_q]=i\hbar\delta_{pq}$ for $p,q=D,1,2,\ldots$ are imposed. For the coordinates of the cavity $\hat{\varphi}_p$ and $\hat{Q}_p$, creation and annihilation operators $\hat{a}_p,\hat{a}_p^\dagger$ are introduced for $p=1,2,\ldots$ according to

$$\hat{Q}_p=\sqrt{\hbar k_pd}\left(\frac{C_0}{L_0}\right)^{1/4}\frac{(\hat{a}_p^\dagger+\hat{a}_p)}{\sqrt{2}}, \qquad \hat{\varphi}_p=i\sqrt{\frac{\hbar}{k_pd}}\left(\frac{L_0}{C_0}\right)^{1/4}\frac{(\hat{a}_p^\dagger-\hat{a}_p)}{\sqrt{2}}. \quad (13)$$

These operators fulfill bosonic commutation relations $[\hat{a}_p,\hat{a}_q^\dagger]=\delta_{pq}$. The Hamiltonian of the isolated dot-cavity system can then be written as

$$\hat{H}_S=\underbrace{\sum_p\hbar\omega_p\hat{a}_p^\dagger\hat{a}_p}_{\hat{H}_C}+\underbrace{\frac{(\hat{Q}_D-C_gV_g)^2}{2C_\Sigma}\left[1+\frac{C^2}{C_\Sigma C_C}\sum_p\zeta_i^2(a)\right]}_{\hat{H}_D} + \underbrace{\frac{C(\hat{Q}_D-C_gV_g)}{C_\Sigma}\sum_p\sqrt{\frac{\hbar\omega_p}{2C_C}}(\hat{a}_p+\hat{a}_p^\dagger)\zeta_p(a)}_{\hat{H}_{DC}}. \quad (14)$$

This Hamiltonian has the desired form $\hat{H}_S=\hat{H}_C+\hat{H}_D+\hat{H}_{DC}$. The first term, $\hat{H}_C$, is the Hamiltonian of a set of harmonic oscillators corresponding to cavity modes with frequencies ω_p. These frequencies are obtained by solving Eq. (8). The second term, $\hat{H}_D$, corresponds to the charging energy of the dot. We see that this is larger than for a dot with self-capacitance C_Σ. The third term in the Hamiltonian, $\hat{H}_{DC}$, is the linear coupling between the charge of the dot and the modes in the cavity. It is convenient for the further analysis to introduce the dimensionless coupling constant

$$\lambda_p=\frac{C}{C_\Sigma}\frac{e\zeta_p(a)}{\sqrt{2\hbar\omega_pC_C}}=\frac{C}{C_\Sigma}\sqrt{\frac{Z_0}{R_q}}\frac{\zeta_p(a)}{\sqrt{k_pd/(2\pi)}}. \quad (15)$$

We emphasize that the Hamiltonian (14) has been obtained in an exact way, without any assumptions about the cavity-dot coupling strength. It is interesting to note, just as was done in Ref. 61, that this exact treatment gives a Caldeira-Leggett type Hamiltonian, naturally including the so-called counter term.[64] This counter term is typically introduced by hand to ensure a spatially uniform damping in the Caldeira-Leggett model. In our model, the counter term just comes from the part of the charging energy term $\hat{H}_D$ arising from the normalization of the capacitance C_Σ.

B. Coupling to leads and Lang-Firsov transformation

As a next step, we consider the tunnel coupling of the dot to external leads L and R. Following the standard path for transport through single-electron transistors,[36] the orbital and charge degrees of freedom of the metallic dot are treated separately. We describe the orbital degrees of freedom by the Hamiltonian

$$\hat{H}_O=\sum_{k'}\epsilon_{Dk'}\hat{c}_{Dk'}^\dagger\hat{c}_{Dk'}, \quad (16)$$

where $\hat{c}_{Dk'}^\dagger$ creates an electron with energy $\epsilon_{Dk'}$ in the dot. The Hamiltonian of the leads is

$$\hat{H}_L=\sum_{\ell,k}\epsilon_{\ell k}\hat{c}_{\ell k}^\dagger\hat{c}_{\ell k}, \quad (17)$$

where $\hat{c}_{\ell k}^\dagger$ is the creation operator of an (uncharged) electron with energy $\epsilon_{\ell k}$ in lead $\ell=L,R$. In Eqs. (16) and (17), the indices k and k' denote both wave number and spin. The tunnel Hamiltonian is written as

$$\hat{H}_T=\sum_{\ell,k,k'}t_{\ell kk'}\hat{c}_{\ell k}^\dagger\hat{c}_{Dk'}\exp\left(\frac{ie\hat{\varphi}_D}{\hbar}\right)+\text{H.c.}, \quad (18)$$

where the operators $\exp(\mp ie\hat{\varphi}_D/\hbar)$ have the effect of changing the dot charge by ±1. This yields a Hamiltonian of the total system

$$\hat{H}=\hat{H}_O+\hat{H}_C+\hat{H}_D+\hat{H}_{DC}+\hat{H}_T+\hat{H}_L. \quad (19)$$

For further analysis, it is convenient to first perform a canonical transformation of $\hat{H}$ that removes the linear-in-charge term $\hat{H}_{DC}$. Such a Lang-Firsov, or polaron,[65] transformation is carried out by transforming the Hamiltonian as $\bar{H}=\exp(\hat{s})\hat{H}\exp(-\hat{s})$ and state kets as $|\bar{\Psi}\rangle=\exp(-\hat{s})|\Psi\rangle$ with

$\hat{s} = [(\hat{Q}_D - C_g V_g)/e] \sum_p \lambda_p (\hat{a}_p^\dagger - \hat{a}_p)$. We then arrive at the Hamiltonian

$$\bar{H} = \hat{H}_L + \hat{H}_O + \sum_p \hbar\omega_p \hat{a}_p^\dagger \hat{a}_p + \frac{(\hat{Q}_D - C_g V_g)^2}{2C_\Sigma} + \sum_{\ell,k,k'} t_{\ell k k'} \hat{c}_{\ell k}^\dagger \hat{c}_{Dk'} \exp\left(\frac{ie\hat{\varphi}_D}{\hbar}\right) \times \exp\left[-\sum_p \lambda_p (\hat{a}_p^\dagger - \hat{a}_p)\right] + \text{H.c.} \quad (20)$$

The eigenstates of the isolated dot-cavity system, decoupled from the leads, are up to an unimportant phase factor given by

$$|N\mathbf{n}\rangle = |N\rangle_{\text{el}} \exp\left[N \sum_p \lambda_p (\hat{a}_p^\dagger - \hat{a}_p)\right] |\mathbf{n}\rangle\,, \quad (21)$$

the tensor product of the charge state with N excess electrons on the dot, $|N\rangle_{\text{el}}$, and the Fock states of the cavity modes, $|\mathbf{n}\rangle = |n_1 n_2 \ldots\rangle$, displaced by $N\lambda_p$ each. We refer to the states $|N\mathbf{n}\rangle$ as microwave polaron states and n_p as the number of photons in mode p. The energies of the polarons are given by

$$\epsilon_{N\mathbf{n}} = \frac{e^2(N - n_g)^2}{2C_\Sigma} + \sum_p n_p \hbar\omega_p \quad (22)$$

with $n_g = C_g V_g/e$. Looking at Eq. (22), we note that the shift in charging energy from the coupling to the cavity modes, a polaron shift, is exactly canceled by the extra charging energy due to the renormalization of the capacitance of the dot. This cancellation is a direct consequence of the exact treatment of the cavity-dot coupling throughout the derivation. If one instead of Eq. (14) naively would start with a standard Anderson-Holstein type Hamiltonian, i.e., without the renormalized capacitance C_Σ, and then perform the polaron transformation, the resulting charging energy term could become negative for large dot-cavity couplings. For a metallic dot with a continuous density of states, such a model would be unphysical; the system would lack a well defined ground state since increasing the number of electrons on the dot always would lower the total energy of the system. It should be noted that problems with infinite negative energies typically do not appear in related electron-phonon models in molecular electronics.[66]

III. QUANTUM MASTER EQUATION

From the Hamiltonian (20), we can then derive a quantum master equation describing the dynamics of both the charge state in the dot and the state of the cavity modes. The derivation follows a standard path, see Refs. 45,67–69.

A. Derivation

In the rest of the paper, we consider the case where the charging energy of the dot, $e^2/(2C_\Sigma)$, is the largest energy in the system. It is then safe to assume that the number of excess electrons on the dot will only fluctuate between N and $N+1$. For simplicity, we consider gate voltages such that N can only take values 0 and 1. The difference in charging energy between states with 0 and 1 electrons is denoted ΔE_C.

Starting from the Liouville equation for the density matrix, expanding to leading order in tunnel coupling and tracing over reservoir and fermionic dot degrees of freedom, we arrive at a quantum master equation for the elements of the reduced density matrix ρ of the dot-cavity system. A more detailed derivation is presented in Appendix A. This equation is in the polaron basis given by

$$\begin{aligned}
\frac{d}{dt}\langle 0\mathbf{n}|\rho|0\mathbf{m}\rangle &= -\frac{i}{\hbar}(\epsilon_{0\mathbf{n}} - \epsilon_{0\mathbf{m}})\langle 0\mathbf{n}|\rho|0\mathbf{m}\rangle + \sum_{\ell,\mathbf{k},\mathbf{l}} \Gamma_\ell [-h_\ell(\epsilon_{1\mathbf{l}} - \epsilon_{0\mathbf{k}}) \prod_p X^p_{k_p l_p} X^p_{m_p l_p} \langle 0\mathbf{n}|\rho|0\mathbf{k}\rangle \\
&\quad + g_\ell(\epsilon_{1\mathbf{l}} - \epsilon_{0\mathbf{m}}) \prod_p X^p_{n_p k_p} X^p_{m_p l_p} \langle 1\mathbf{k}|\rho|1\mathbf{l}\rangle + g_\ell(\epsilon_{1\mathbf{k}} - \epsilon_{0\mathbf{n}}) \prod_p X^p_{n_p k_p} X^p_{m_p l_p} \langle 1\mathbf{k}|\rho|1\mathbf{l}\rangle \\
&\quad - h_\ell(\epsilon_{1\mathbf{k}} - \epsilon_{0\mathbf{l}}) \prod_p X^p_{n_p k_p} X^p_{l_p k_p} \langle 0\mathbf{l}|\rho|0\mathbf{m}\rangle], \\
\frac{d}{dt}\langle 1\mathbf{n}|\rho|1\mathbf{m}\rangle &= -\frac{i}{\hbar}(\epsilon_{1\mathbf{n}} - \epsilon_{1\mathbf{m}})\langle 1\mathbf{n}|\rho|1\mathbf{m}\rangle + \sum_{\ell,\mathbf{k},\mathbf{l}} \Gamma_\ell [-g_\ell(\epsilon_{1\mathbf{k}} - \epsilon_{0\mathbf{l}}) \prod_p X^p_{l_p k_p} X^p_{l_p m_p} \langle 1\mathbf{n}|\rho|1\mathbf{k}\rangle \\
&\quad + h_\ell(\epsilon_{1\mathbf{m}} - \epsilon_{0\mathbf{l}}) \prod_p X^p_{k_p n_p} X^p_{l_p m_p} \langle 0\mathbf{k}|\rho|0\mathbf{l}\rangle + h_\ell(\epsilon_{1\mathbf{n}} - \epsilon_{0\mathbf{k}}) \prod_p X^p_{k_p n_p} X^p_{l_p m_p} \langle 0\mathbf{k}|\rho|0\mathbf{l}\rangle \\
&\quad - g_\ell(\epsilon_{1\mathbf{l}} - \epsilon_{0\mathbf{k}}) \prod_p X^p_{k_p n_p} X^p_{k_p l_p} \langle 1\mathbf{l}|\rho|1\mathbf{m}\rangle], \quad (23)
\end{aligned}$$

where $h_\ell(x) = [x - (\mu_\ell - \mu_D)]/(\hbar\omega_1)(\exp\{[x - (\mu_\ell - \mu_D)]/k_B T\} - 1)^{-1}$, $g_\ell(x) = \exp\{[x - (\mu_\ell - \mu_D)]/k_B T\} h_\ell(x)$, and $\Gamma_\ell = 2\pi |t_\ell|^2 \nu_\ell \nu_D \omega_1$. Here, μ_ℓ and μ_D are the chemical potentials of the leads and the dot, respectively. Moreover, we have assumed tunneling amplitudes independent of lead and dot energy, i.e., $t_{kk'\ell} \approx t_\ell$ and ν_ℓ and ν_D denotes the density of states of lead ℓ and the dot, respectively. Furthermore,

$$X^p_{nm} = \langle n| \exp[-\lambda_p(\hat{a}_p^\dagger - \hat{a}_p)]|m\rangle = \frac{1}{\sqrt{m!}} e^{-\lambda_p^2/2} \sum_{j=0}^{\min(m,n)} \lambda_p^{n+m-2j} (-1)^{n-j} \binom{m}{j} \frac{\sqrt{n!}}{(n-j)!} \quad (24)$$

are the Franck-Condon factors[65] for the pth mode. These are the amplitudes for the transition from the state in mode p going between polaron states with n and m quanta as the electron tunnels into or our of the dot. Formally, X^p_{nm} is given by the overlap of oscillator wave functions before and after the tunneling. We emphasize that Eq. (23) is a quantum master equation: it describes the dynamics of the polaron states as well as coherences between them.

B. Franck-Condon effect

From Eq. (24), we note that for all Franck-Condon factors, $X^p_{nm} \propto \exp(-\lambda_p^2/2)$. This means that even if no photons are excited as the electrons tunnel into and out of the dot, $n = m = 0$, the presence of the modes in the cavity will still affect transport via renormalized, suppressed tunneling rates. This Franck-Condon suppression of electron tunneling is a pure vacuum effect, a consequence of the tunneling charge having to displace all the oscillators in the cavity. We introduce the vacuum renormalized tunneling rates:

$$\tilde{\Gamma}_\ell = \Theta\Gamma_\ell, \quad \Theta = \exp\left(-\sum_p \lambda_p^2\right), \tag{25}$$

where Θ denotes the renormalization factor. It is convenient to also introduce the notation $Y^p_{nm} = \exp(\lambda_p^2/2)X^p_{nm}$ for the remaining part of the Franck-Condon factors for the pth mode.

From Eq. (15), it follows that the coupling constant λ_p is proportional to $\zeta_p(a)/\sqrt{k_p d}$. Consequently [see Eqs. (7) and (8)], the renormalization factor depends on the the distance a and the parameter $\alpha = CC_g/(C_\Sigma C_C)$. Since the dot can be placed at any position a, or effectively be moved by tuning the boundary conditions of the cavity,[19,70] it is interesting to study the position dependence of Θ, plotted in Fig. 2 for different values of α. Several observations can be made: (i) albeit the renormalization factor can be large, it is always finite for $\alpha > 0$. There is thus no tunneling orthogonality catastrophe, i.e., zero overlap between initial and final states in a tunneling event. Such an orthogonality catastrophe would occur if one naively replaces $\zeta_p(a)$ and k_p with the corresponding amplitude $\sqrt{2/d}\cos(p\pi a/d)$ and wave number $p\pi/d$ of the cavity disconnected from the dot. The exponent of the renormalization factor would then be proportional to $\sum_p \cos(p\pi/d)^2/p$, which diverges logarithmically. We emphasize that it is our exact treatment of the dot charge-cavity coupling fully taking into account the effect of the presence of the dot on the cavity modes that gives a finite $\tilde{\Gamma}_\ell$. (ii) We see that the renormalization factor has a strong dependence on the distance a, with a minimum at $a = d/2$ and maximum at $a = 0$. This is a consequence of that all modes have maximal amplitude $\zeta_p(a)$ at $a = d$, while at $a = d/2$, half of the modes, i.e., the antisymmetric, will have zero amplitude. (iii) We note that Θ decreases with decreasing α. This is to be expected, since a small α means that the amplitude of the cavity modes at the connection point remains finite for higher frequencies. It is also interesting to point out that a position dependence of the coupling constant was very recently investigated in the context of nanoelectromechanical systems.[71,72]

C. Parameter regime

The quantum master equation (23) allows us to investigate the charge and photon dynamics in a broad range of parameters. The main interest of the present work is to investigate new physical phenomena becoming important for strong dot-cavity coupling. This motivates us to focus on the deep quantum regime, with only a few photons in the cavity, where these phenomena can be investigated both qualitatively and quantitatively. Spelling out explicitly the parameter range, we consider symmetric tunnel couplings, $\Gamma_L = \Gamma_R = \Gamma$, and a symmetric bias $\mu_L = -\mu_R = \mathrm{eV}/2$, giving a chemical potential of the dot $\mu_D = 0$. We also consider the case where only the two lowest photon modes have finite populations. This restriction puts limits on the bias voltage; a careful investigation gives that $|\mathrm{eV}/2 \pm \Delta E_C| < \hbar\omega_2$ is necessary to guarantee a negligible occupation of the third and higher modes in all cases of interest. This condition means that it is energetically forbidden for a tunneling electron to emit a photon directly into the second mode. However, population of the second mode is still possible by intermode conversion of photons from the first mode, as discussed below. In the rest of the article, we will use the simplified notation $|Nn_1n_2\rangle$ for the polaron states with $N = 0,1$ electrons and n_1,n_2 photons in the first and second mode, respectively.

We further assume that the tunneling rate is much smaller than the fundamental cavity frequency, i.e., $\tilde{\Gamma} \ll \omega_1$. For the case where only the first photon mode is active, the off-diagonal elements $\langle \mu n_1 0|\rho|\mu m_1 0\rangle$ with $n_1 \neq m_1$ of the steady-state density matrix in Eq. (23) are a factor $\sim\tilde{\Gamma}/\omega_1 \ll 1$ smaller than the diagonal elements and can be disregarded. This amounts to performing a secular, or rotating-wave, approximation and reduces Eq. (23) to a standard master equation. For two active modes, the situation is different since two polaron states $|Nn_1n_2\rangle$ and $|Nm_1m_2\rangle$ can be degenerate, i.e., for $n_1\omega_1 + n_2\omega_2 - (m_1\omega_1 + m_2\omega_2) \ll \tilde{\Gamma}$, the secular approximation can not be performed. The off-diagonal density matrix elements $\langle Nn_1n_2|\rho|Nm_1m_2\rangle$, corresponding to coherences between polaron states with different number of photons, must thus be retained in Eq. (23). The simplest case giving degeneracy, discussed in detail below, occurs for $\alpha \ll 1$ when from Eq. (8) $\omega_2 \approx 2\omega_1$. Moreover, to highlight the effect of the coherences, we compare in several cases below the results based on Eq. (23) to the results based on a master equation where the off-diagonal elements are disregarded from the outset.

A key parameter in our work is the coupling constant λ_1. To reach the strong-coupling regime, the time scale for tunnel-induced excitation and relaxation of the cavity photons must be much shorter than the intrinsic relaxation time. This amounts to the restriction

$$\sqrt{\kappa/\tilde{\Gamma}} \ll \lambda_1, \tag{26}$$

on the coupling constant, where $\kappa = \omega_1/(2\pi Q)$ is the intrinsic relaxation rate of the first cavity mode and Q is the quality factor. To provide a concrete estimate, for reasonable parameters of a superconducting transmission line cavity $\omega_1/2\pi = 10$ GHz, $Q = 10^6$, $Z_0 = 100\ \Omega$, and $C \sim C_\Sigma$, one has $\kappa = 10$ kHz and $\lambda_1 = 0.06$. Then, for a tunneling rate

$\tilde{\Gamma} = 200$ MHz, the left-hand side of Eq. (26) is an order of magnitude smaller than the right-hand side.

The ultrastrong regime requires the coupling constant λ_1 to be of order unity. For the capacitive dot-cavity coupling considered here, it has however been pointed out[3,73] that standard superconducting transmission lines only allow couplings λ_1 up to a few percent. The limiting factor, clear from Eq. (15), is the ratio $Z_0/R_q \ll 1$. To reach larger couplings, one thus has to consider ways of increasing the characteristic impedance Z_0 of the transmission line. One promising possibility is transmission lines with a central conductor consisting of an array of Josephson junctions or SQUIDs acting as linear inductors. In recent experiments with SQUID array conductors,[57,58] $Z_0 \approx 6\,\mathrm{k}\Omega$, i.e., $Z_0/R_q \approx 0.25$, was demonstrated, which would correspond to λ_1 of the order of tens of percent for a dot capacitively coupled to the transmission line. It should, however, be pointed out that in such high impedance transmission lines, nonlinear effects, not accounted for in our model, start to become relevant.

The relation between the coupling constants λ_1 and λ_2 is determined by Eqs. (15) and (8) as

$$\frac{\lambda_2}{\lambda_1} \approx \frac{\cos(2\pi a/d)}{\cos(\pi a/d)}, \tag{27}$$

for $\alpha \ll 1$. This relation is thus specified by a. Below we will consider two important qualitatively distinct cases, $a = d/4$ and and $a = 0$. For $a = d/4$, we have $\lambda_2 = 0$ and only a the first mode has finite population. The case $a = 0$ corresponds to a position in the cavity yielding maximal coupling strength. Equation (27) then gives $\lambda_1 = \sqrt{2}\lambda_2$ and both the first and the second modes can have finite population.

IV. STATE OF THE PHOTON MODES OF THE CAVITY

We first consider the current-induced photon state in the cavity, the electronic transport is considered below. Experimentally, the photon state in the cavity can, for example, be investigated by capacitively coupling the cavity to a transmission line and measuring the state of the output itinerant modes.[74] This gives access to the frequency-resolved population[29] as well as higher moments of the cavity field via, for example, quantum-state tomography of one[75] or two[76] itinerant modes. Moreover, the photon number[77] as well as the full photon state,[15] can also be obtained by coupling the cavity to a superconducting qubit embedded in the cavity. Studying specific experimental setups to extract information about the photon state is, however, out of the scope of the present article. Hence we concentrate on the photon state of the cavity described by the steady-state density matrix obtained from Eq. (23).

A. Single-mode

We first consider the case of a single active mode obtained when the coupling strength for the second mode is zero, i.e., $\lambda_2 = 0$. To demonstrate the effect of the tunneling electrons on the state of the first mode, it is instructive to consider the average number of photon excitations in the two polaron states, $n_{\mathrm{ph}} = \sum_n n P_n$ with $P_n = \langle 0n0|\rho_s|0n0\rangle + \langle 1n0|\rho_s|1n0\rangle$ and ρ_s is the steady-state density matrix. The average number

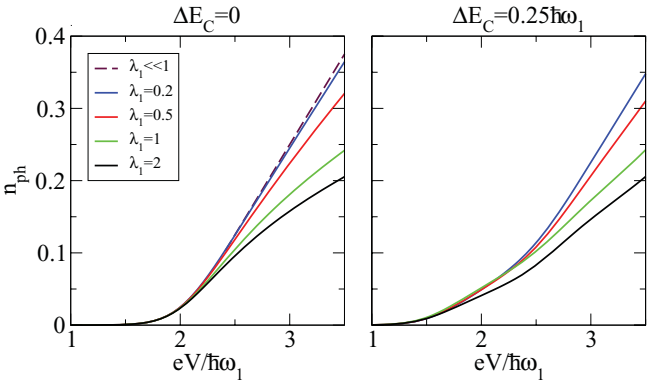

FIG. 3. (Color online) Mean number of photon excitations n_{ph} for a single active mode ($\lambda_2 = 0$) as a function of bias voltage eV for different coupling strengths λ_1 and charging energy differences $\Delta E_C = 0$ (left) and $0.25\hbar\omega_1$ (right). The temperature is $k_B T = 0.05\hbar\omega_1$. In the left panel, the dashed line gives the analytical result Eq. (30) for $\mathrm{eV} - 2\hbar\omega_1 \gg k_B T$.

of excitations n_{ph} is related to the photon population in the unrotated basis $\langle \hat{n}_1 \rangle$ as $\langle \hat{n}_1 \rangle = n_{\mathrm{ph}} + \lambda_1^2 \sum_n \langle 1n0|\rho_s|1n0\rangle$. In Fig. 3, n_{ph} is plotted against the bias voltage for different coupling strengths λ_1. Considering the curves corresponding to charge degeneracy, i.e., $\Delta E_C = 0$, we note that n_{ph} is zero until the bias voltage eV reaches $2\hbar\omega_1$ after which it starts to increase continuously with bias voltage. For the curves corresponding to $\Delta E_C = 0.25\hbar\omega_1$, the onset occurs at $\mathrm{eV} = 1.5\hbar\omega_1$ and there is an additional kink on each curve at $\mathrm{eV} = 2.5\hbar\omega_1$.

These onsets and kinks can be understood from the energetics of allowed tunneling processes: due to the continuous density of states of the dot, all electrons in the lead with energies above ΔE_C can tunnel into the dot. Photon emission by the tunneling electrons is, however, only possible for electrons with energies above $\hbar\omega_1 + \Delta E_C$. Similarly, an electron in the dot can tunnel out to unoccupied states in the leads with energies below ΔE_C, but can only tunnel out with photon emission to states with energies below $\Delta E_C - \hbar\omega_1$. Therefore, at low temperatures, photon emission is only possible by an electron tunneling from (to) the left (right) lead for a bias voltages $\mathrm{eV}/2 \gtrsim \hbar\omega_1 + (-)\Delta E_C/2$. The onsets and kinks in Fig. 3 thus correspond to thresholds of tunneling processes with photon emission into the cavity.

The rate of increase of the population n_{ph} with increasing $\mathrm{eV} > 2\hbar\omega_1 - \Delta E_C$ can most easily be understood for $\Delta E_c = 0$. We see in Fig. 3 that the population goes from growing almost linearly for $\lambda_1 = 0.2$ to a slower, sublinear increase for larger $\lambda_1 \sim 1$. In the limit $\lambda_1 \ll 1$, an analytical formula for the photon distribution $\{P_n\}$ can be derived by only taking into account processes to leading order in λ_1 (see Appendix C). For $\mathrm{eV} - 2\hbar\omega_1 \gg k_B T$, we obtain

$$P_n = \frac{2\hbar\omega_1}{\mathrm{eV} + 2\hbar\omega_1} \left(\frac{\mathrm{eV} - 2\hbar\omega_1}{\mathrm{eV} + 2\hbar\omega_1} \right)^n, \tag{28}$$

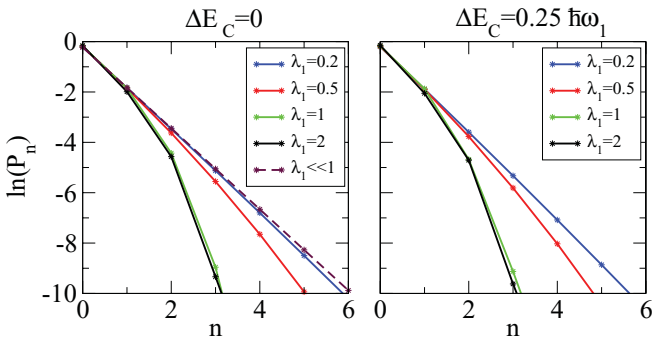

FIG. 4. (Color online) Logarithm of the probability of n photons for different coupling strengths and $\Delta E_C = 0$ (left) and $\Delta E_C = 0.25\hbar\omega_1$ (right) for bias voltage $\mathrm{eV} = 3\hbar\omega_1$ and $k_BT = 0.05\hbar\omega_1$.

independent of λ_1. We note that the probabilities P_n are Boltzmann distributed. Hence the distribution can be described by an effective temperature

$$k_B T_{\mathrm{eff}} = \hbar\omega_1 / \ln[(\mathrm{eV} + 2\hbar\omega_1)/(\mathrm{eV} - 2\hbar\omega_1)]. \quad (29)$$

Using standard thermodynamics, we then obtain the following linear relation between the population and bias voltage as

$$n_{\mathrm{ph}} = \frac{1}{\exp(\hbar\omega_1/[k_B T_{\mathrm{eff}}]) - 1} = \frac{\mathrm{eV} - 2\hbar\omega_1}{4\hbar\omega_1}. \quad (30)$$

Looking at Fig. 3, we see that n_{ph} is well described by Eq. (30) for coupling strengths up to $\lambda_1 \approx 0.2$. The slower increase with voltage for larger λ_1 can be understood as follows: in the limit $\lambda_1 \ll 1$, only processes where the number of photons is changed -1, 0, or 1 are important, since they are the only ones having nonzero amplitude to leading order in λ_1. This is deduced from the corresponding Franck-Condon factors [see Eq. (24)]. However, at the considered bias voltages, only processes where the number of photons is *increased* by at most one are allowed energetically. Thus when λ_1 is increased, the rate for the higher-order processes where the photons number is *decreased* becomes larger, but not for the ones where the photon number is increased. Hence the population n_{ph} is decreased. The results are qualitatively similar for $\Delta E_C = 0.25\hbar\omega_1$.

To further investigate the properties of the distribution, $\{P_n\}$ for coupling strengths approaching $\lambda_1 \sim 1$, P_n is plotted against n for bias $\mathrm{eV} = 3\hbar\omega_1$ in Fig. 4. We see that the distribution decreases exponentially with n for couplings $\lambda_1 \ll 1$ in line with Eq. (28). For stronger couplings, the decrease is faster due to higher-order relaxation processes. This observation shows that the probabilities P_n are not Boltzmann distributed and hence an effective temperature cannot be defined. The cavity mode is thus clearly in a nonthermal state. This can be further illustrated by investigating, for example, the photon Fano factor[53] (not presented here).

An important feature of the photon state, not captured in the above analysis, is that an electron tunneling into the dot displaces the harmonic oscillator corresponding to the first cavity mode by an amount proportional to the coupling

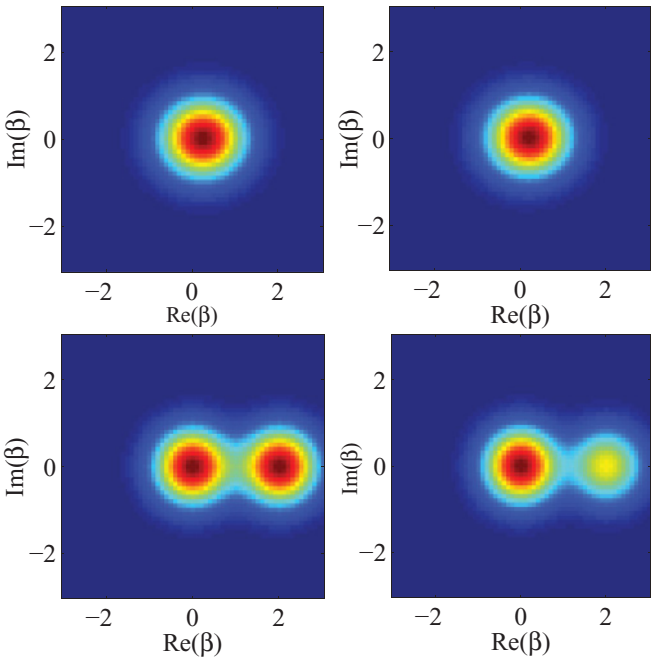

FIG. 5. (Color online) Wigner function $W(\beta)$ for coupling strengths $\lambda_1 = 0.2$ (upper panel) and 2 (lower panel) and charging energy differences $\Delta E_C = 0$ (left) and $0.25\hbar\omega_1$ (right). The color scale goes from blue (small value) to red (large value). The bias voltage is $\mathrm{eV} = 3\hbar\omega_1$ and the temperature is $k_BT = 0.05\hbar\omega_1$.

strength, λ_1. To illustrate the effect of the displacement of the mode, we plot in Fig. 5 the Wigner-function[78]

$$W(\beta) = \int \frac{d^2\xi}{\pi} \mathrm{tr}[\rho_s \exp(\xi \hat{a}_1^\dagger - \xi^* \hat{a}_1)] \exp(\xi\beta^* - \xi^*\beta), \quad (31)$$

where the trace is taken over both electron and photon degrees of freedom. From Fig. 5, we note that for coupling $\lambda_1 = 0.2$, we can only discern a single peak of the Wigner function, while for the larger coupling, $\lambda_1 = 2$, the peak is split into two. The second peak comes from the photons of the polaron of the charged dot and it becomes visible for coupling strengths $\lambda_1 \sim 1$. We also note that ΔE_C has an impact on the photon distribution as the second peak is weaker for $\Delta E_C = 0.25\hbar\omega_1$ than for $\Delta E_C = 0$. This is a consequence of a smaller probability of the dot being occupied in the previous case.

It is interesting to briefly compare our results to those obtained for the sequential tunneling current-induced nonequilibrium state of a single-boson mode coupled to a single level, see, e.g., Refs. 45,51,55 and 79. For a single-level dot, in contrast to our metallic dot, the population grows stepwise with bias voltage, where each step corresponds to an onset of photon emission in a tunneling process. Furthermore, in contrast to our result (30), the photon distribution and hence the population is not convergent for charge degeneracy, $\Delta E_C = 0$, in the limit of couplings, $\lambda_1 \ll 1$, for voltages above the first onset of photon emission.[51,55] This is because the rate for going from a state with n to a state with $n+1$ photons is equal to the rate for the opposite process, which gives an equal probability of all photon states. In metallic dot, the processes $n+1 \to n$ has larger rate than

$n \to n+1$, as discussed in detail in Appendix C. We note, however, that in single-level systems, where higher-order tunneling processes become important, the boson distribution is found to be convergent.[45] See also recent works, e.g., Refs. 80–83.

B. Two active modes

We then turn to the case with two active modes with $\lambda_1 = \sqrt{2}\lambda_2$. As for the single-mode case, we first consider the average number of photon excitations in the two polaron states, defined by $n_{\mathrm{ph1(2)}} = \sum_{n,m} n(m)(\langle 0nm|\rho_s|0nm\rangle + \langle 1nm|\rho_s|1nm\rangle)$. The dependence of n_{ph1} and n_{ph2} on bias voltage for different coupling strengths is depicted in Fig. 6. We see that the onsets and slopes in the curves for n_{ph1} show the same qualitative behavior as in the single-mode case. Moreover, importantly, n_{ph2} have onsets and kinks at the same bias voltages. This is despite the fact that direct excitation of this mode is not energetically allowed at the considered bias voltages. The population in the second mode is thus due to *intermode conversion*. The mechanism of this conversion is that a tunneling electron excites a photon in the second mode and simultaneously deexcites a photon in the first mode. Since the change of the energy of the tunneling electron is the same as when it emits a photon into the first mode, both processes become energetically allowed at the same bias voltage. We note from Fig. 6 that n_{ph2} initially increases with $\lambda_1 = 1$ up to and starts to decrease again for even large $\lambda_1 = 2$. We also point out that there is a difference between the results obtained from calculations with and without the coherences retained. This is particularly apparent for the coupling strength $\lambda_1 = 1$. Here, n_{ph1} and n_{ph2} are larger and significantly larger, respectively, in the presence of coherences. To identify the dependence of the coherent effects on the coupling strengths, we plot the difference between the coherent and the incoherent

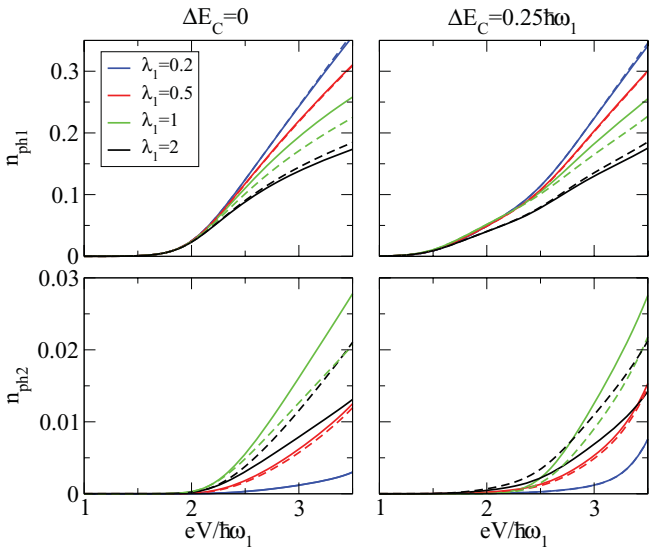

FIG. 6. (Color online) Mean number of photons in first and second modes, n_{ph1} and n_{ph2}, against bias voltage for different coupling strengths and ΔE_C. The temperature is $k_B T = 0.05\hbar\omega_1$. Solid (dashed) lines show results with (without) coherences retained.

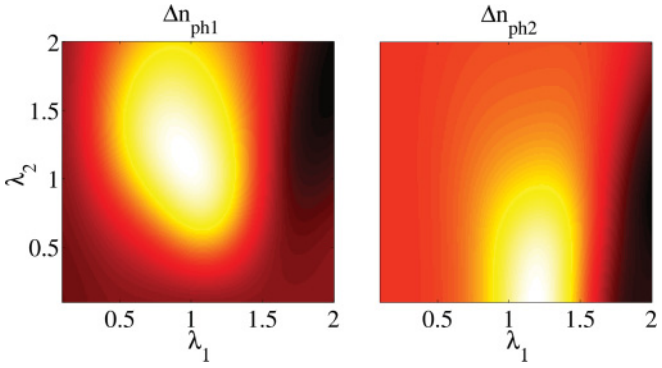

FIG. 7. (Color online) The difference between the obtained average number of excitations in the first n_{ph1} (left) and second n_{ph2} (right) modes when coherences are retained and not in the quantum master equation. The color scale goes from black (small difference) to white (large difference). The bias voltage is $\mathrm{eV} = 3\hbar\omega_1$ and temperature is $k_B T = 0.05\hbar\omega_1$.

occupations n_{ph1} and n_{ph2} as a function of λ_1 and λ_2 for bias voltage $\mathrm{eV} = 3\hbar\omega_1$ in Fig. 7.

1. Polaron coherences

As is clear from both Figs. 6 and 7, the effect of coherences on n_{ph1} and n_{ph2} are most pronounced around $\lambda_1 = 1$ for which they are enhanced. For the coupling strength to the second mode, the effect of the coherence is maximal around $\lambda_2 \sim 1$ for n_{ph1}, while the effect on n_{ph2} is maximal for $\lambda_2 \ll 1$. To qualitatively understand the origin of the coherences, we compare transition between low-energy states for the coherent and incoherent cases. The transitions between states with an energy in the cavity modes less or equal to $\hbar\omega_1$ are the same both in the presence and absence of coherence. For transitions to, from, or between states with an energy $2\hbar\omega_1$ in the cavity modes, however, the picture is different. Consider, for example, the transition from $|110\rangle$ in which an additional quanta $\hbar\omega_1$ is excited in the cavity modes. Two processes contribute to this transition: an additional photon can be excited in the first mode, $|110\rangle \to |020\rangle$, and a photon can be excited in the second mode by intermode conversion $|110\rangle \to |001\rangle$. Since $|020\rangle$ and $|001\rangle$ are degenerate, the final state is a superposition of them in the coherent case, while there is no superposition in the incoherent case. Similar explanations hold for the other transitions to, from, or between states with energy $2\hbar\omega_1$.

To provide a simple physical picture illustrating the effect of the coherences, we perform a detailed investigation of the quantum master equation in Eq. (23) for the representative pair of couplings $\lambda_1 = 1$ and $\lambda_2 = 1/\sqrt{2}$, giving large coherence effects. As shown in Appendix D, we find that for states with an energy $2\hbar\omega_1$ in the cavity modes only two superpositions,

$$|0\Omega\rangle = \frac{|020\rangle + |001\rangle}{\sqrt{2}}, \quad |1\Phi\rangle = \frac{|120\rangle - |101\rangle}{\sqrt{2}}, \quad (32)$$

have non-negligble populations. Moreover, for the considered bias voltages, transitions to and from states with an energy larger than $2\hbar\omega_1$ in the cavity modes can be neglected. This

allows us to describe the charge and photon properties by an effective master equation

$$\frac{d\mathbf{P}}{dt} = M\mathbf{P}, \tag{33}$$

where $\mathbf{P} = [P_{000}, P_{010}, P_{0\Omega}, P_{100}, P_{110}, P_{1\Phi}]^T$, with $P_{\mu 00}, P_{\mu 10}$, $P_{0\Omega}$, and $P_{1\Phi}$ being the probabilities for the states $|\mu 00\rangle$, $|\mu 10\rangle$, $|0\Omega\rangle$, and $|1\Phi\rangle$, respectively. The matrix M in Eq. (33) is further given by

$$M/\tilde{\Gamma} = \begin{pmatrix} -\sum_{j=0,1}\tilde{h}_j & 0 & 0 & \tilde{g}_0 & \tilde{g}_1 & 0 \\ 0 & -\sum_{j=-1,1}\tilde{h}_j & 0 & \tilde{g}_{-1} & 0 & \tilde{g}_1 \\ 0 & 0 & -\sum_{j=-1,0}\tilde{h}_j & 0 & \tilde{g}_{-1} & \tilde{g}_0 \\ \tilde{h}_0 & \tilde{h}_{-1} & 0 & -\sum_{j=0,-1}\tilde{g}_j & 0 & 0 \\ \tilde{h}_1 & 0 & \tilde{h}_{-1} & 0 & -\sum_{j=-1,1}\tilde{g}_j & 0 \\ 0 & \tilde{h}_1 & \tilde{h}_0 & 0 & 0 & -\sum_{j=0,1}\tilde{g}_j \end{pmatrix}, \tag{34}$$

where $\tilde{h}_j = \sum_{\ell=L,R} h_\ell(j\hbar\omega_1 + \Delta E_C)$ and $\tilde{g}_j = \sum_{\ell=L,R} g_\ell(j\hbar\omega_1 + \Delta E_C)$.

The transitions described by Eq. (33) are depicted in Fig. 8 along with the transitions of the corresponding incoherent master equation with probabilities $P_{\mu 00}$, $P_{\mu 10}$, $P_{\mu 20}$, and $P_{\mu 01}$. We see that one major difference between the coherent and incoherent master equation is that there is no direct relaxation from states with energy $2\hbar\omega_1$ to states with zero energy in the photon modes in the coherent case (see Appendix D). This coherent blocking of relaxation provides a plausible explanation of why $n_{\rm ph1}$ and $n_{\rm ph2}$ are enhanced in the coherent case (see Fig. 6).

Moreover, an expression for the steady-state density matrix, ρ_s, can be obtained from Eq. (33). Considering $\Delta E_C = 0$ and $\mathrm{eV} - 2\hbar\omega_1 \gg k_B T$, the steady-state density matrix has the simple form

$$\begin{aligned}\rho_s = {} & \frac{1}{2}\frac{1}{3(\mathrm{eV})^2 + 4(\hbar\omega_1)^2} \\ & \times \{(|000\rangle\langle 000| + |100\rangle\langle 100|)(\mathrm{eV} + 2\hbar\omega_1)^2 \\ & + (|010\rangle\langle 010| + |110\rangle\langle 110|)[(\mathrm{eV})^2 - 4(\hbar\omega_1)^2] \\ & + (|0\Omega\rangle\langle 0\Omega| + |1\Phi\rangle\langle 1\Phi|)(\mathrm{eV} - 2\hbar\omega_1)^2\}. \end{aligned} \tag{35}$$

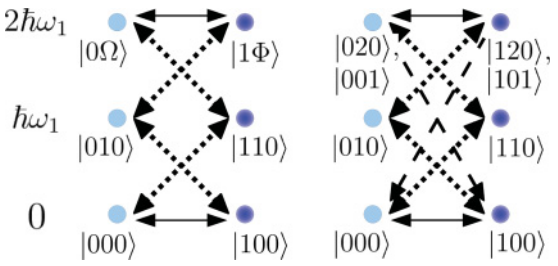

FIG. 8. (Color online) Scheme of transition between different states for the effective master equation (33) (left) and the corresponding incoherent master equation (right). The filled lines represents transitions when no photon is emitted or absorbed and the dotted lines represent transitions involving one photon. The dashed lines represents transitions where two photons are emitted.

This expression clearly shows that the superpositions of polaron states have finite probabilities. The steady-state density matrix thus displays nontrivial correlations between the cavity photon state and the charge state of the dot. From Eq. (35), we also find that the populations

$$\begin{aligned} n_{\rm ph1} &= \frac{2\mathrm{eV}(\mathrm{eV} - 2\hbar\omega_1)}{3(\mathrm{eV})^2 + 4(\hbar\omega_1)^2} \\ n_{\rm ph2} &= \frac{1}{2}\frac{(\mathrm{eV} - 2\hbar\omega_1)^2}{3(\mathrm{eV})^2 + 4(\hbar\omega_1)^2}, \end{aligned} \tag{36}$$

are in good agreement with the numerical results in Fig. 6.

V. ELECTRONIC TRANSPORT AND NOISE

Having investigated the current-induced nonequilibrium photon state, we now turn to the properties of the electronic transport itself, fully accounting for the back action of the cavity photons on the tunneling electrons. We focus our investigation on the average current and the low-frequency current fluctuations, or noise,[84] experimentally accessible in metallic quantum dots.[85] The current I and the noise S can conveniently be calculated from the number-resolved version of the quantum master equation (23), as discussed in the context of full counting statistics, see, e.g., early works[86–89] for a detailed discussion. For completeness of the present work, we give in Appendix B a short derivation of the expressions for the current and the noise, used in the analytical and numerical calculations below.

A. Conductance and noise for a single active mode

We first consider the I-V characteristics when only a single mode is active, i.e., $\lambda_2 = 0$. In Fig. 9, the conductance $G = dI/dV$ is plotted against bias voltage for different coupling strengths and charging energy differences ΔE_C. The main feature of the conductance is a stepwise increase as the bias voltage passes $2\hbar\omega_1$ and $(2 \pm 0.5)\hbar\omega_1$ for $\Delta E_C = 0$ and $\Delta E_C = 0.25\hbar\omega_1$, respectively. As concluded in the last section, at these bias voltages, photon emission in the tunneling

process becomes energetically allowed. In the low-bias regime, $eV < 2\hbar\omega_1 - \Delta E_C$, the cavity modes affect the transport only by renormalizing the tunneling rate [Franck-Condon effect, see Eq. (25)]. Considering specifically $\Delta E_C = 0$, the conductance is

$$G_0 = \frac{e^2\tilde{\Gamma}}{4\hbar\omega_1} \tag{37}$$

for any λ_1. For $eV > 2\hbar\omega_1$, the electrons can also tunnel by emitting or absorbing a photon in the first mode. Thus additional transport channels open up, which gives the increase in conductance. For $\lambda_1 \ll 1$, an analytical formula can be derived for the conductance (see Appendix C). For bias voltages $eV - 2\hbar\omega_1 \gg k_BT$, the conductance is given by

$$G_1 = \frac{e^2\tilde{\Gamma}\left(1+\lambda_1^2\right)}{4\hbar\omega_1}. \tag{38}$$

Thus the contribution from the additional channels scales as λ_1^2. This dependence derives from the rate of emission or absorption of one photon in a tunneling event proportional to $|Y^1_{nn+1}|^2 \propto \lambda_1^2$. Interestingly, the result in Eq. (38) is independent on the distribution $\{P_n\}$. For larger coupling strengths, $\lambda_1 \sim 1$, processes of higher order in λ_1 start to contribute to the conductance and Eq. (38) no longer holds. The rate of tunneling into and out of the dot will be dependent on the number of photons in the cavity, i.e., the conductance becomes dependent on the distribution $\{P_n\}$. As is seen in Fig. 9, the higher-order processes typically lead to an increased conductance.

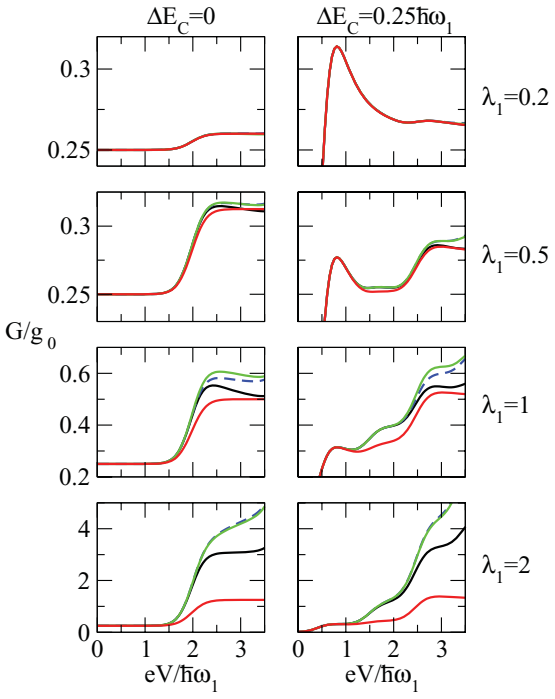

FIG. 9. (Color online) Differential conductance as a function of bias voltage, in units of $g_0 = e^2\tilde{\Gamma}/\hbar\omega_1$. The results are obtained by a quantum master equation for one mode (black), two modes without coherences (dashed blue), two modes with coherences (green), and for an equilibrated photon distribution at temperature $k_BT_{\rm ph} \ll \hbar\omega_1$ (red). The electron temperature was $k_BT = 0.05\hbar\omega_1$.

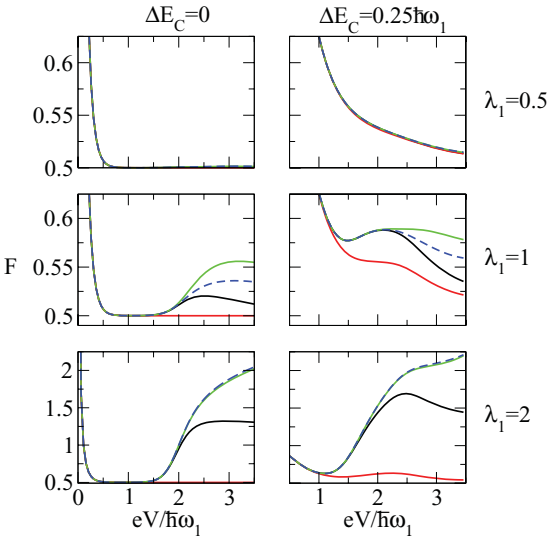

FIG. 10. (Color online) Fano factor as a function of bias voltage obtained for one mode (black), two modes without coherences (dashed blue), two modes with coherences (green), and for the first mode being equilibrated (red). The temperature was $k_BT = 0.05\,\hbar\omega_1$.

To gain further insight into the effect of the coupling to the photon mode on the electron transport properties, we investigate the correlations between the tunneling electrons. The correlations are quantified by the Fano factor $F = S/(eI)$. For a dot decoupled from the cavity, the electrons are anticorrelated due to the Coulomb interaction, and F is always less than one for bias voltage $eV - \Delta E_C \gg k_BT$. The Fano factor for the dot coupled to a single photon mode is plotted against bias voltage in Fig. 10. Below the onset voltage, the only effect of the coupling between the dot and the cavity mode is a renormalization of the tunneling rates. Focusing on $\Delta E_C = 0$, the noise is

$$S = \frac{e^3V\tilde{\Gamma}}{8\hbar\omega_1}, \tag{39}$$

giving a Fano factor of 1/2. Above onset, i.e., for bias voltages $eV - 2\hbar\omega_1 \gg k_BT$, the noise becomes dependent on the coupling strength λ_1. In the limit $\lambda_1 \ll 1$, an expression for the noise can be found analytically (See Appendix C). We find

$$S = \frac{e^2\tilde{\Gamma}}{4\hbar\omega_1}\left[\frac{eV\left(1+\lambda_1^2\right)}{2\hbar\omega_1} - \lambda_1^2\right] = \frac{eI}{2}, \tag{40}$$

which gives a Fano factor of 1/2 above the onset voltage as well. Thus the onset of photon emission does not change the correlations between the tunneling electrons. We point out that corrections to the Fano factor in Eq. (40) are of order λ_1^4. Consequently, as can be seen in Fig. 10, the deviation in the Fano factor from 1/2 for $\Delta E_C = 0$ is small even for coupling strengths as large as $\lambda_1 = 0.5$. However, for coupling strengths approaching $\lambda_1 \sim 1$, we see an increase in the Fano factor as the bias voltage passes $2\,\hbar\omega_1$ and for $\lambda_1 = 2$, we even get super-Poissonian noise. Similarly, we see for $\Delta E_C = 0.25\,\hbar\omega_1$ that there is an increase in the Fano factor for the bias voltage $1.5\,\hbar\omega_1$ for coupling strengths $\lambda_1 \sim 1$.

Thus the change in the Fano factor above the onset voltage occurs for coupling strengths deep into the ultrastrong coupling regime, $\lambda_1 \sim 1$. To understand this, we recall that the tunneling into and out of the dot is dependent on the photon state for these coupling strengths. For two subsequently tunneling electrons, this means that the tunneling rate for the later electron depends on which photon state the cavity mode was left in by the first electron. For the parameter regime investigated, this leads to an increased tendency of bunching, and hence a larger Fano factor. In an equivalent physical picture, the increase in the Fano factor can be attributed to the emergence of the avalanche effect found for a single level strongly coupled to a boson mode described in Ref. 48. We thus find that the effect is also present for a metallic dot coupled to a boson mode.

To highlight the effect of the nonequilibrium photon distribution on the transport properties, it is instructive to compare the result presented above to ones where the cavity modes are equilibrated at $T_{\rm ph}$. (See Appendix E for details.) To keep the discussion short, we focus the discussion on temperatures $T_{\rm ph}$ for which only the first mode can have a finite thermal population and $\Delta E_C = 0$. We consider first the conductance $G^{\rm th}$ and restate that for coupling strengths $\lambda_1 \ll 1$, the conductance is independent on the photon distribution. Hence the conductance for an equilibrated mode is given by Eqs. (37) and (38) below and above the onset voltage, respectively. For larger coupling strengths, $\lambda_1 \sim 1$, when the photon distribution affects the transport, the conductances for equilibrated and nonequilibrated modes differ. For bias voltages below the onset voltage, the conductance is given by

$$G_0^{\rm th} = \frac{e^2\tilde{\Gamma}}{4\hbar\omega_1}\exp\left\{-\lambda_1^2\left[\coth\left(\frac{\hbar\omega_1}{2k_BT_{\rm ph}}\right)-1\right]\right\} \times\sum_{n=0}^{\infty}(2-\delta_{n0})\exp\left(\frac{-n\hbar\omega_1}{2k_BT_{\rm ph}}\right) \times I_n\left[\lambda_1^2\sinh^{-1}\left(\frac{\hbar\omega_1}{2k_BT_{\rm ph}}\right)\right]. \quad (41)$$

Here, I_n denotes the nth order modified Bessel function of the first kind. The conductance in Eq. (41) is an increasing function of the temperature and it is thus larger than than the conductance in Eq. (37). For bias voltages above the onset voltage, the conductance for the equilibrated mode is given by $G_1^{\rm th} = G_0^{\rm th} + \Delta G^{\rm th}$ with

$$\Delta G^{\rm th} = \frac{e^2\tilde{\Gamma}}{4\hbar\omega_1}\exp\left\{-\lambda_1^2\left[\coth\left(\frac{\hbar\omega_1}{2k_BT_{\rm ph}}\right)-1\right]\right\} \times 2\sinh\left(\frac{\hbar\omega_1}{2k_BT_{\rm ph}}\right)I_1\left[\lambda_1^2\sinh^{-1}\left(\frac{\hbar\omega_1}{2k_BT_{\rm ph}}\right)\right]. \quad (42)$$

For $k_BT_{\rm ph} \ll \hbar\omega_1$, the expression for $G_1^{\rm th}$ reduces to Eq. (38), obtained for a nonequilibrium photon distribution in the limit $\lambda_1 \ll 1$.

It can be shown (see Appendix E) that $\Delta G^{\rm th}/G_0^{\rm th}$ is limited by the low-temperature value λ_1^2. Importantly, for the nonequilibrium photon mode investigated above, the relative difference in conductance $\Delta G/G_0$ in Fig. 9 is not limited to λ_1^2. To clearly illustrate the difference between the conductances for thermalized and nonequilibrium modes, $G^{\rm th}$ is plotted as a reference in Fig. 9.

Further insight is obtained by comparing the Fano factors for equilibrated and nonequilibrated modes. For an equilibrated mode, we find (see Appendix E) that in the low-temperature limit, $k_BT_{\rm ph} \ll \hbar\omega_1$, for arbitrary couplings λ_1 and $\Delta E_C = 0$, the noise is given by Eqs. (39) and (40) below and above the onset voltage, respectively. The low-temperature Fano factors are plotted as a reference in Fig. 10. For finite temperatures, the expressions for the noise below and above the onset voltage are lengthy and do not provide additional physical insight. We therefore simply provide the qualitative result: the Fano factor decays monotonically with bias voltage for a given $T_{\rm ph}$. As is clear from Fig. 10 and the discussion above, the later result is in contrast to what we find for a nonequilibrium photon distribution. The increase in the Fano factor at the onset voltage for ultrastrong couplings, $\lambda_1 \sim 1$, is thus a clear signature of a nonequilibrium photon distribution of the cavity mode.

B. Conductance and noise for two active modes

We then turn to the transport properties for the case with two active modes, with couplings $\lambda_1 = \sqrt{2}\lambda_2$. The differential conductance and the Fano factor are plotted against bias in Figs. 9 and 10 for both the cases with and the cases without coherences retained in the quantum master equation. As for a single active mode, there is a stepwise increase in differential conductance as the bias voltage approaches $2\hbar\omega_1$ and $2\hbar\omega_1 \pm 0.5\hbar\omega_1$ for $\Delta E_C = 0$ and $\Delta E_C = 0.25\hbar\omega_1$, respectively. We note that the conductance is typically larger than for the single-mode case for a given coupling strength λ_1. Thus the intermode conversion, discussed in the last section, typically increases the conductance. Similarly, there is an increase in the Fano factor at the onset voltage.

We note that there is a difference between the conductance obtained when coherences are included in the master equation and not. The difference is most apparent for $\lambda_1 = 1$, where they lead to enhancement of the conductance. This agrees with the finding that $n_{\rm ph1}$ and $n_{\rm ph2}$ show the most pronounced effect of the coherences around this coupling strength (depicted in Figs. 6 and 7). We recall from the previous section that processes where the energy in the photon modes is decreased by more than $\hbar\omega_1$ are blocked when coherences are retained in the master equation for $\lambda_1 = 1$. We attribute the conductance enhancement to this blocking effect since the blocked processes contribute to transfer of electrons in the opposite direction to the applied bias. We also see that the effect of the coherences on the Fano factor shows the most pronounced effect at coupling strengths $\lambda_1 \sim 1$. It is interesting to note that in a very recent work on nanoelectromechanical systems,[90] the conductance of a few-level quantum dot coupled to several vibrational modes was investigated incorporating the effects of coherence between degenerate vibrational states.

VI. CONCLUSIONS

In conclusion, we have investigated theoretically the properties of a metallic quantum dot strongly coupled to a superconducting transmission line cavity. The focus of the investigations has been on the interplay between the cavity photon state and the electronic transport through the dot. Based

on the Lagrangian formulation of circuit QED, a Hamiltonian for the system was derived for arbitrary strong dot-cavity coupling. The electronic transport and the photon dynamics were described by a quantum master equation fully accounting for coherent and nonequilibrium photon effects. The cases with one and two active photon modes were investigated. For a single active mode strongly coupled to the conduction electrons, the photon state was found to be nonequilibrium, with clear signatures of microwave polaron formation. For two active modes, coherence and photon conversion between the two modes was found. Turning to the transport, the effect of the nonequilibrium photon state on the electronic conduction was investigated by comparing to the results for an equilibrated photon mode. Clear transport signatures due to the nonequilibrium photon distribution were found, in particular, super-Poissonian shot noise for strong dot-cavity couplings.

ACKNOWLEDGMENTS

We thank Göran Johansson, Takis Kontos, Per Delsing, Klaus Ensslin, Kohnrad Lehnert, and Olov Karlström for fruitful discussions and input. The work was supported by the Swedish VR. We also thank Federica Haupt, Maura Sassetti, Fabio Cavaliere, Gianluca Rastelli, and Christian Flindt for constructive comments on an earlier version of the manuscript.

APPENDIX A: DERIVATION OF QUANTUM MASTER EQUATION

The time evolution of the system is given by the Liouville equation $\partial_t \hat{\rho} = -\frac{i}{\hbar}[H_T(t), \hat{\rho}(t)]$, where $\hat{\rho}$ is the interaction picture density operator of the system. For weak tunnel coupling considered here, we can restrict the analysis to the sequential tunneling regime (Born approximation). We first expand the Liouville equation to second order in the tunnel coupling giving

$$\frac{d\hat{\rho}}{dt} = -\frac{i}{\hbar}[H_T(t), \hat{\rho}(\tau)] - \frac{1}{\hbar^2}\int_\tau^t dt' \{H_T(t), [H_T(t'), \hat{\rho}(t)]\}. \tag{A1}$$

Then the decoupled density operator $\hat{\rho} = \hat{\rho}_L \otimes \hat{\rho}_O \otimes \hat{\rho}_S$ is inserted. Here, $\hat{\rho}_L$, $\hat{\rho}_O$, and $\hat{\rho}_S$ are the density operators of the leads, the fermionic degrees of freedom of the dot and the dot charge-cavity system, respectively. Taking the dot and the leads to be in thermal equilibrium, we can trace Eq. (A1) over the lead and fermionic dot degrees of freedom. Further, performing a Markov approximation and letting $\tau \to -\infty$, Eq. (23) is obtained for the matrix elements of the Schrödinger picture reduced density operator ρ in the polaron basis. We point out that coherences between states with 0 and 1 electrons in the dot are not considered since they do not couple to the elements in Eq. (23), diagonal with respect to the charge degree of freedom.[36,67]

APPENDIX B: CURRENT, NOISE AND FULL COUNTING STATISTICS

The starting point for the derivation of the current and and low-frequency noise is the expression for the cumulant generating function $F(\chi)$. The cumulant generating function is given by the logarithm of the Fourier transform of the distribution of probabilities $P(N,t)$ to transfer N electrons through the dot during a measurement time t, as $t\,F(\chi) = -\ln[\sum_N P(N,t)\exp(iN\chi)]$. The different cumulants of the charge transfer are obtained by successive differentiation of $F(\chi)$ with respect to the counting field χ. The first two cumulants are the current I and noise S given by $I = e(-i\partial_\chi)F(\chi)|_{\chi=0}$ and $S = e^2(-i\partial_\chi)^2 F(\chi)|_{\chi=0}$, respectively.

To arrive at $F(\chi)$ in our model, we first write the N-resolved version of the quantum master equation (23) on a vectorized form. After Fourier transformation with respect to N we then get the equation $d\boldsymbol{\rho}(\chi)/dt = M(\chi)\boldsymbol{\rho}(\chi)$. The cumulant generating function is given by the eigenvalue of $M(\chi)$ that goes to zero for $\chi = 0$. For our purposes, to obtain explicit expressions for the different cumulants, the generating function can conveniently be written as the solution to the eigenvalue equation

$$M(\chi)\boldsymbol{\rho}(\chi) = F(\chi)\boldsymbol{\rho}(\chi). \tag{B1}$$

We then expand all quantities in χ as $F(\chi) = (i\chi/e)I + (i\chi/e)^2 S/2 + \ldots$, $M(\chi) = M_0 + i\chi M_1 + \ldots.$, and $\boldsymbol{\rho}(\chi) = \boldsymbol{\rho}^{(0)} + i\chi\boldsymbol{\rho}^{(1)} + \ldots$, which inserted into Eq. (B1) gives a hierarchy of coupled linear equations as

$$\begin{aligned} M^{(0)}\boldsymbol{\rho}^{(0)} &= 0, \\ M^{(0)}\boldsymbol{\rho}^{(1)} + M^{(1)}\boldsymbol{\rho}^{(0)} &= I\boldsymbol{\rho}^{(0)}, \\ M^{(0)}\boldsymbol{\rho}^{(2)} + M^{(1)}\boldsymbol{\rho}^{(1)} + M^{(2)}\boldsymbol{\rho}^{(0)} &= I\boldsymbol{\rho}^{(1)} + S\boldsymbol{\rho}^{(0)}/2, \ldots \end{aligned} \tag{B2}$$

The zeroth order equation gives the steady-state density matrix $\boldsymbol{\rho}^{(0)}$. Expressions for the higher-order $\boldsymbol{\rho}^{(n)}$ are obtained by combining the nth and lower-order equations. By multiplying the first- and higher-order equations from the left with the left zero eigenvector $\mathbf{v}$ of $M^{(0)}$, defined from $\mathbf{v}^T M^{(0)} = 0$, inserting the expression for $\rho^{(n)}$, and imposing the normalization condition $\mathbf{v}^T\boldsymbol{\rho}^{(0)} = 1$, the different cumulants are obtained. These equations are then solved numerically and, in some limiting cases, analytically (see, e.g., Appendix C). For the numerical evaluation, it is convenient to follow Ref. 91 and fix the single free parameter in $\boldsymbol{\rho}^{(n)}$, the component parallel to $\boldsymbol{\rho}^{(0)}$, by imposing a suitable normalization of $\boldsymbol{\rho}^{(n)}$. Formally, the first two cumulants, current and noise, can be written as[91]

$$\begin{aligned} I &= e\mathbf{v}^T M^{(1)}\boldsymbol{\rho}^{(0)}, \\ S &= eI - 2e^2\mathbf{v}^T M^{(1)} R M^{(1)}\boldsymbol{\rho}^{(0)}, \end{aligned} \tag{B3}$$

where R denotes the pseudoinverse of the singular matrix $M^{(0)}$ and we used $M^{(2)} = M^{(1)}/2$.

APPENDIX C: DERIVATION, $\lambda_1 \ll 1$ LIMIT

We here present the derivation of analytical formulas for the photon distribution, the current and the noise for a single cavity mode coupled to the dot in the limit $\lambda_1 \ll 1$, for charge degeneracy, $\Delta E_c = 0$. Performing the secular approximation on Eq. (23) the following standard master equation, including

counting fields (see Appendix B), is obtained

$$\sum_\ell \begin{pmatrix} M_\ell^{00} & M_\ell^{10} e^{i\chi_\ell} \\ M_\ell^{01} e^{-i\chi_\ell} & M_\ell^{11} \end{pmatrix} \begin{pmatrix} \mathbf{P}_0(\chi) \\ \mathbf{P}_1(\chi) \end{pmatrix} = F(\chi) \begin{pmatrix} \mathbf{P}_0(\chi) \\ \mathbf{P}_1(\chi) \end{pmatrix}, \tag{C1}$$

where $\ell = L,R$, $\chi_L = 0$, and $\chi_R = \chi$. Here, $\mathbf{P}_0(\chi) = [\langle 000|\rho(\chi)|000\rangle, \langle 010|\rho(\chi)|010\rangle \dots]^T$ and $\mathbf{P}_1(\chi) = [\langle 100|\rho(\chi)|100\rangle, \langle 110|\rho(\chi)|110\rangle \dots]^T$ are vectors corresponding to 0 or 1 electrons on the dot, and the elements of the M_ℓ matrices are given by

$$\begin{aligned} \left(M_\ell^{00}\right)_{nm} &= -\delta_{nm}\tilde{\Gamma} \sum_{k=-1}^{1} \left|Y^1_{n(n+k)}\right|^2 h_\ell(k\hbar\omega_1), \\ \left(M_\ell^{11}\right)_{nm} &= -\delta_{nm}\tilde{\Gamma} \sum_{k=-1}^{1} \left|Y^1_{n(n+k)}\right|^2 g_\ell(k\hbar\omega_1), \\ \left(M_\ell^{10}\right)_{nm} &= \tilde{\Gamma} \sum_{k=-1}^{1} \delta_{n(m-k)} \left|Y^1_{n(n+k)}\right|^2 g_\ell(k\hbar\omega_1), \\ \left(M_\ell^{01}\right)_{nm} &= \tilde{\Gamma} \sum_{k=-1}^{1} \delta_{n(m-k)} \left|Y^1_{n(n+k)}\right|^2 h_\ell(k\hbar\omega_1), \end{aligned} \tag{C2}$$

where the renormalized Franck-Condon factors Y^1_{nm} are defined below Eq. (2). Here, terms up to second order in λ_1 are kept in $|Y^1_{nm}|^2$ (only $|Y^1_{nm}|^2$ with $m = n, n \pm 1$ contribute). By expanding Eq. (C1) to zeroth order in χ the equation for the steady state, probabilities $\mathbf{P}_0^{(0)}$ and $\mathbf{P}_1^{(0)}$ are recovered. Since $h_R(x) = g_L(-x)$ and $h_L(x) = g_R(-x)$, we have $M^{00}_{L(R)} = M^{11}_{R(L)}$ and $M^{01}_{L(R)} = M^{10}_{R(L)}$. The equations for $\mathbf{P}_0^{(0)}$ and $\mathbf{P}_1^{(0)}$ are thus symmetric, and we can write $\mathbf{P}_0^{(0)} = \mathbf{P}_1^{(0)} = \mathbf{P}^{(0)}$ and obtain the following equation for $P_n^{(0)} = (\mathbf{P}^{(0)})_n$ as

$$\begin{aligned} \sum_\ell \Big\{ &-\left[\left|Y^1_{nn-1}\right|^2 h_\ell(-\hbar\omega_1) + \left|Y^1_{nn+1}\right|^2 h_\ell(\hbar\omega_1)\right] P_n^{(0)} \\ &+ \left|Y^1_{nn+1}\right|^2 h_\ell(-\hbar\omega_1) P_{n+1}^{(0)} + \left|Y^1_{nn-1}\right|^2 h_\ell(\hbar\omega_1) P_{n-1}^{(0)} \Big\} = 0, \end{aligned} \tag{C3}$$

on the same form as found in Ref. 45. This equation has the solution

$$P_n^{(0)} = \frac{(1-\eta)\eta^n}{2} \tag{C4}$$

with $\eta = [\sum_\ell h_\ell(\hbar\omega_1)/\sum_\ell h_\ell(-\hbar\omega_1)]$ and where we have imposed the normalization condition $2\sum_n P_n^{(0)} = 1$. We point out that despite the expression being independent on λ_1 it is correct to order λ_1^2. For $\mathrm{eV} - 2\hbar\omega_1 \gg k_BT$, we have $\eta = (\mathrm{eV} - 2\hbar\omega_1)/(\mathrm{eV} + 2\hbar\omega_1)$ giving Eq. (28). (Note that in the main text, we use P_n for $P_n^{(0)}$ for notational convenience.) We also note that η is the ratio between the rates of electron tunneling with photon emission and tunneling with photon absorption. This ratio is always smaller than one, which ensures that the distribution is convergent.

The current is calculated according to Eq. (B3). For $\mathrm{eV} - 2\hbar\omega_1 \gg k_BT$, this gives

$$\begin{aligned} I = e\tilde{\Gamma} \sum_n \Bigg[&\underbrace{n\lambda_1^2 \frac{\mathrm{eV} + 2\hbar\omega_1}{2\hbar\omega_1}}_{\Gamma_{n\uparrow}/\tilde{\Gamma}} + \underbrace{\left(1 - 2n\lambda_1^2\right)\frac{\mathrm{eV}}{2\hbar\omega}}_{\Gamma_{n0}/\tilde{\Gamma}} \\ &+ \underbrace{(n+1)\lambda_1^2 \frac{\mathrm{eV} - 2\hbar\omega_1}{2\hbar\omega_1}}_{\Gamma_{n\downarrow}/\tilde{\Gamma}} \Bigg] \end{aligned}$$

$$P_n^{(0)} = \frac{e\tilde{\Gamma}}{2} \left[\frac{\mathrm{eV}\left(1 + \lambda_1^2\right)}{2\hbar\omega_1} - \lambda_1^2 \right]. \tag{C5}$$

From this equation Eq. (38) follows directly. Furthermore, the expression allows us to identify the contributions $\Gamma_{n\downarrow}$, Γ_{n0}, and $\Gamma_{n\uparrow}$ to the total rate for tunneling into/out of the dot in a state with n photons. We see from Eq. (C5) that the rates for absorbing $\Gamma_{n\downarrow}$ or emitting a photon $\Gamma_{n\uparrow}$ in the tunneling process increases with n. This increase is, however, canceled by an equally large decrease in the rate for tunneling without photon emission or absorption Γ_{n0}. This cancellation makes the effective rate independent of n. The current will therefore be independent on the distribution $\{P_n^{(0)}\}$.

The noise can most conveniently be obtained from the expression for the generating function $F(\chi)$. Above onset, for $\mathrm{eV} - 2\hbar\omega_1 \gg k_BT$, there is no tunneling against the bias and the matrices $M_L^{10}, M_R^{01}, M_L^{11}$, and M_R^{00} in Eq. (C1) can be neglected. Using the symmetries of the M_ℓ matrices, we can then write Eq. (C1) as

$$\begin{pmatrix} M_R^{00} & M_R^{10} e^{i\chi} \\ M_R^{10} & M_R^{00} \end{pmatrix} \begin{pmatrix} \mathbf{P}_0(\chi) \\ \mathbf{P}_1(\chi) \end{pmatrix} = F(\chi) \begin{pmatrix} \mathbf{P}_0(\chi) \\ \mathbf{P}_1(\chi) \end{pmatrix}. \tag{C6}$$

From Eq. (C5) together with the expression for the current in Eq. (B3), it is clear that $e\tilde{v}^T M_R^{10} \mathbf{P}^{(0)} = 2I\tilde{v}^T \mathbf{P}^{(0)} = I$, where $\tilde{v}^T = [1,1,1,\dots]$ and the normalization condition $\tilde{v}^T \mathbf{P}^{(0)} = 1/2$. Since the current is independent on $\mathbf{P}^{(0)}$, we have $\tilde{v}^T M_R^{10} = (2I/e)\tilde{v}^T$, i.e., $\tilde{v}^T$ is the left eigenvector to M_R^{10} with eigenvalue $2I/e$. Moreover, from Eq. (C3) for $\mathbf{P}^{(0)}$, we can write $\tilde{v}^T(M_R^{00} + M_R^{10}) = 0$, i.e., $\tilde{v}^T M_R^{00} = -\tilde{v}^T M_R^{10} = -(2I/e)\tilde{v}^T$. Multiplying both sides of Eq. (C6) from the left by $[\tilde{v}^T, \tilde{v}^T]$, then gives

$$\frac{2I}{e} \begin{pmatrix} -1 & e^{i\chi} \\ 1 & -1 \end{pmatrix} \begin{pmatrix} \tilde{v}^T \mathbf{P}_0(\chi) \\ \tilde{v}^T \mathbf{P}_1(\chi) \end{pmatrix} = F(\chi) \begin{pmatrix} \tilde{v}^T \mathbf{P}_0(\chi) \\ \tilde{v}^T \mathbf{P}_1(\chi) \end{pmatrix}. \tag{C7}$$

This 2×2 eigenvalue equation is directly solved, giving the cumulant generating function

$$F(\chi) = \frac{2I}{e}(e^{i\chi/2} - 1). \tag{C8}$$

From this expression we have, following Appendix B, the current I and the noise $S = eI/2$, the expression in Eq. (40).

APPENDIX D: EFFECTIVE MASTER EQUATION

We here present a derivation of the effective master equation (33). In particular, we explain why only the coherences (32)

appear in this equation. As a starting point, we consider the transitions from the state $|010\rangle$ in which an additional quanta $\hbar\omega_1$ is excited. As stated in the main text, the final state is a superposition of the states $|120\rangle$ and $|101\rangle$. We change the basis of the corresponding degenerate subspace to $\{|1\Phi\rangle, |1\Omega\rangle\}$, with

$$|1\Phi\rangle = \frac{Y_{12}^1 Y_{00}^2 |120\rangle + Y_{10}^1 Y_{01}^2 |101\rangle}{\sqrt{\left|Y_{12}^1 Y_{00}^2\right|^2 + \left|Y_{10}^1 Y_{01}^2\right|^2}},$$
$$|1\Omega\rangle = \frac{Y_{10}^1 Y_{01}^2 |120\rangle - Y_{12}^1 Y_{00}^2 |101\rangle}{\sqrt{\left|Y_{12}^1 Y_{00}^2\right|^2 + \left|Y_{10}^1 Y_{01}^2\right|^2}}, \tag{D1}$$

where $Y_{lm}^p = \exp(\lambda_p^2/2) X_{lm}^p$ are the reduced Franck-Condon factors. From Eq. (23), we find that the amplitude for the transition $\langle 010|\rho|010\rangle \to \langle 1\Phi|\rho|1\Phi\rangle$ is finite, while the amplitude for $\langle 010|\rho|010\rangle \to \langle 1\Omega|\rho|1\Omega\rangle$ is zero. Similarly, we find by changing the basis in the subspace $\{|020\rangle, |001\rangle\}$ to

$$|0\Omega\rangle = \frac{-Y_{21}^1 Y_{00}^2 |020\rangle - Y_{01}^1 Y_{10}^2 |001\rangle}{\sqrt{\left|Y_{21}^1 Y_{00}^2\right|^2 + \left|Y_{01}^1 Y_{10}^2\right|^2}},$$
$$|0\Phi\rangle = \frac{Y_{01}^1 Y_{10}^2 |020\rangle - Y_{21}^1 Y_{00}^2 |001\rangle}{\sqrt{\left|Y_{21}^1 Y_{00}^2\right|^2 + \left|Y_{01}^1 Y_{10}^2\right|^2}} \tag{D2}$$

that the transition $\langle 110|\rho|110\rangle \to \langle 0\Omega|\rho|0\Omega\rangle$ has finite amplitude, while the amplitude for the transition $\langle 110|\rho|110\rangle \to \langle 0\Phi|\rho|0\Phi\rangle$ is zero. Thus, if the system is in the state $|110\rangle$ ($|010\rangle$) prior to the tunneling event with excitation of a quantum $\hbar\omega_1$, the final state is $|0\Omega\rangle$ ($|1\Phi\rangle$).

For the considered bias voltages and coupling strengths, the occupations of the states with energy larger than $2\hbar\omega_1$ in the cavity modes is negligibly small. Moreover, transitions from $|000\rangle$ to $|1\Omega\rangle$ and $|1\Phi\rangle$ and from $|100\rangle$ to $|0\Phi\rangle$ and $|0\Omega\rangle$ are energetically forbidden. Considering finally transitions between states with energy $2\hbar\omega_1$ in the cavity modes, we find for the specific choice of coupling strengths $\lambda_1 = \sqrt{2}\lambda_2 = 1$, (but not in general) that the amplitudes for the transition $\langle 1\Phi|\rho|1\Phi\rangle \leftrightarrow \langle 0\Phi|\rho|0\Phi\rangle$ and $\langle 0\Omega|\rho|0\Omega\rangle \leftrightarrow \langle 1\Omega|\rho|1\Omega\rangle$ vanish. This shows conclusively that the states $|0\Phi\rangle$ and $|1\Omega\rangle$ decouple from the other states in the quantum master equation and that an effective master equation can be written in terms off the occupation probabilities of the states $\{|000\rangle, |100\rangle, |010\rangle, |110\rangle, |0\Omega\rangle, |1\Phi\rangle\}$, i.e., Eq. (33). Inserting $\lambda_1 = \sqrt{2}\lambda_1 = 1$ into Eqs. (D1) and (D2), we find that the states $|0\Omega\rangle$ and $|1\Phi\rangle$ are given by Eq. (32). We also note that transitions $\langle 1\Phi|\rho|1\Phi\rangle \to \langle 0\Omega|\rho|0\Omega\rangle$ and $\langle 0\Omega|\rho|0\Omega\rangle \to \langle 100|\rho|100\rangle$ have zero amplitude. This explains the blocking of relaxation from states with energy $2\hbar\omega_1$ to states with zero energy in the cavity modes discussed in the main text.

APPENDIX E: THERMALIZED CAVITY MODES

We here present how the conductance and noise are calculated in the case of equilibrated cavity modes at a temperature $T_{\rm ph}$. Most of the results presented in this section are available in the existing literature.[36] They are included here merely for completeness of the paper and to facilitate the comparison to the nonequilibrium case.

The starting point for obtaining the conductance and noise for thermally equilibrated modes is to derive a master equation for the charge degree of freedom only. This derivation is to a large part identical to the one presented in Appendix A. However, the density operator $\hat{\rho}_S$ in Eq. (A1) is assumed to factorize into $\hat{\rho}_D \otimes \hat{\rho}_{\rm ph}$, where $\hat{\rho}_D$ and $\hat{\rho}_{\rm ph}$ are the density operators of the charge degree of freedom and the thermally distributed photons, respectively. Further, additional partial trace is taken over the photon degrees of freedom. The following master equation for the diagonal elements P_0 and P_1 of $\hat{\rho}_D$ is then obtained:

$$\frac{d}{dt}\begin{pmatrix} P_0 \\ P_1 \end{pmatrix} = \begin{pmatrix} -\Gamma_{01} & \Gamma_{10} \\ \Gamma_{01} & -\Gamma_{10} \end{pmatrix}\begin{pmatrix} P_0 \\ P_1 \end{pmatrix}. \tag{E1}$$

The rates $\Gamma_{01} = \Gamma_{01}^+ + \Gamma_{01}^-$ and $\Gamma_{10} = \Gamma_{10}^+ + \Gamma_{10}^-$, where $\Gamma_{01(10)}^{\pm}$ is the rate to tunnel in (+) or opposite to (−) the direction of the applied bias, from 0 to 1 (1 to 0) excess charges on the dot, given by

$$\Gamma_{01(10)}^{\pm} = \frac{\tilde{\Gamma}}{\hbar\omega_1}\int_{-\infty}^{\infty} dE dE' f(E)[1 - f(E')] \times \tilde{P}\left[E - E' \pm \frac{\rm eV}{2} - (+)\Delta E_C\right], \tag{E2}$$

where $\tilde{P}(E) = \exp(\sum_p \lambda_p^2) P(E)$ and

$$P(E) = \frac{1}{2\pi\hbar}\int_{-\infty}^{\infty} dt \exp\left(\frac{iEt}{\hbar}\right)\prod_p \langle [\hat{X}^p(t)]^\dagger \hat{X}^p(0)\rangle, \tag{E3}$$

with

$$\hat{X}^p(t) = \exp[-\lambda_p(\hat{a}_p^\dagger e^{i\omega t} - \hat{a}_p e^{-i\omega t})]. \tag{E4}$$

The function $P(E)$ is interpreted as the probability for an electron to emit a net energy E in to the cavity modes in the tunneling event. This approach for studying tunneling in the presence of an equilibrated electromagnetic environment is commonly referred to as $P(E)$ theory.[36] $\tilde{P}(E)$ can be written as

$$\tilde{P}(E) = \sum_{\{n_p\}} \delta\left(E - \sum_p n_p \hbar\omega_p\right)\prod_p \tilde{P}_{n_p}^p, \tag{E5}$$

with

$$\tilde{P}_n^p = \exp\left\{\frac{n\hbar\omega_p}{2k_B T_{\rm ph}} - \lambda_p^2\left[\coth\left(\frac{\hbar\omega_p}{2k_B T_{\rm ph}}\right) - 1\right]\right\} \times I_n\left\{\lambda_p^2/\sinh[\hbar\omega_p/(2k_B T_{\rm ph})]\right\}, \tag{E6}$$

where I_n is the nth order modified Bessel function of the first kind.[36]

From Eq. (E1), the current and noise can now be obtained from Eq. (B1) as

$$I^{\rm th} = \frac{e(\Gamma_{10}^+\Gamma_{01}^+ - \Gamma_{10}^-\Gamma_{01}^-)}{\Gamma_{01}^+ + \Gamma_{01}^- + \Gamma_{10}^- + \Gamma_{10}^+},$$
$$S^{\rm th} = \frac{e^2(\Gamma_{10}^+\Gamma_{01}^+ + \Gamma_{10}^-\Gamma_{01}^-)}{\Gamma_{01}^+ + \Gamma_{01}^- + \Gamma_{10}^- + \Gamma_{10}^+} - \frac{2e^2(\Gamma_{10}^+\Gamma_{01}^+ - \Gamma_{10}^-\Gamma_{01}^-)^2}{(\Gamma_{01}^+ + \Gamma_{01}^- + \Gamma_{10}^- + \Gamma_{10}^+)^3}. \tag{E7}$$

These expression are used to obtain the plots in Figs. 9 and 10.

For charge degeneracy, $\Delta E_C = 0$, the formula for the current simplifies to $I^{\rm th} = e(\Gamma_{01}^+ - \Gamma_{01}^-)/2$. This can be used to

derive Eqs. (41) and (42). Considering temperatures such that only the first mode has a finite population, the current below onset $I_0^{\rm th}$ and above onset $I_1^{\rm th}$ are given in terms of $\tilde{P}_n^1$ by

$$I_0^{\rm th} = \frac{e^2 V\tilde{\Gamma}}{4\hbar\omega_1}\left(\tilde{P}_0^1 + 2\sum_{n=1}^{\infty}\tilde{P}_{-n}^1\right),$$
$$I_1^{\rm th} = \frac{e^2 V\tilde{\Gamma}}{4\hbar\omega_1}\left(\sum_{n=-1}^{1}\frac{{\rm eV}-2n\hbar\omega_1}{\rm eV}\tilde{P}_n^1 + 2\sum_{n=2}^{\infty}\tilde{P}_{-n}^1\right). \quad \text{(E8)}$$

For temperatures $k_B T_{\rm ph} \ll \hbar\omega_1$, we have $\tilde{P}_0^1 = 1, \tilde{P}_1^1 = \lambda_1^2$, and $\tilde{P}_n^1$ with $n \leqslant -1$ exponentially suppressed. Then Eq. (E8) gives Eqs. (41) and (42). We also note that from Eq. (E8), we have

$$\frac{\Delta G^{\rm th}}{G_0^{\rm th}} = \frac{\tilde{P}_1^1 - \tilde{P}_{-1}^1}{\tilde{P}_0^1 + 2\sum_{n=1}^{\infty}\tilde{P}_{-n}^1} \leqslant \frac{\tilde{P}_1^1 - \tilde{P}_{-1}^1}{\tilde{P}_0^1}$$
$$= \frac{2\sinh\left(\frac{\hbar\omega_1}{2k_B T_{\rm ph}}\right) I_1\left[\lambda_1^2/\sinh\left(\frac{\hbar\omega_1}{2k_B T_{\rm ph}}\right)\right]}{I_0\left[\lambda_1^2/\sinh\left(\frac{\hbar\omega_1}{2k_B T_{\rm ph}}\right)\right]} \leqslant \lambda_1^2, \quad \text{(E9)}$$

where $\Delta G^{\rm th} = G_1^{\rm th} - G_0^{\rm th}$. The conductance step $\Delta G^{\rm th}/G_0^{\rm th}$ is thus limited above by λ_1^2.

For charge degeneracy, $\Delta E_C = 0$, the expression for the noise simplifies to $S^{\rm th} = e^2(\Gamma_{01}^+ + \Gamma_{01}^-)/4$. For temperatures such that only the first mode has a finite population, the noise below $S_0^{\rm th}$ and above $S_1^{\rm th}$ onset can be written as

$$S_0^{\rm th} = \frac{e^2}{8\hbar\omega_1}\left({\rm eV}\tilde{P}_0^1 + \sum_{n=1}^{\infty}4n\hbar\omega_1\tilde{P}_{-n}^1\right),$$
$$S_1^{\rm th} = \frac{e^2}{8\hbar\omega_1}\left[\sum_{n=-1}^{1}({\rm eV}-2n\hbar\omega_1)\tilde{P}_n^1 + \sum_{n=2}^{\infty}4n\hbar\omega_1\tilde{P}_{-n}^1\right]. \quad \text{(E10)}$$

For temperatures $k_B T_{\rm ph} \ll \hbar\omega_1$, these formulas reduce to Eqs. (39) and (40). It is clear from Eqs. (E8) and (E10) that the thermal Fano factors $F_0^{\rm th} = S_0^{\rm th}/(eI_0^{\rm th})$ and $F_1^{\rm th} = S_1^{\rm th}/(eI_1^{\rm th})$ decreases monotonically with bias voltage and that $F_1^{\rm th} < F_0^{\rm th}$. Hence the Fano factor decreases monotonically with bias voltage.

[1] A. Blais, R. S. Huang, A. Wallraff, S. M. Girvin, and R. J. Schoelkopf, Phys. Rev. A **69**, 062320 (2004).
[2] A. Wallraff, D. Schuster, A. Blais, L. Frunzio, R. Huang, J. Majer, S. Kumar, S. Girvin, and R. Schoelkopf, Nature (London) **431**, 162 (2004).
[3] R. Schoelkopf and S. Girvin, Nature (London) **451**, 664 (2008).
[4] M. Sillanpää, J. Park, and R. Simmonds, Nature (London) **449**, 438 (2007).
[5] J. Majer *et al.*, Nature (London) **449**, 443 (2007).
[6] L. DiCarlo *et al.*, Nature (London) **460**, 240 (2009).
[7] L. DiCarlo, M. Reed, L. Sun, B. Johnson, J. Chow, J. Gambetta, L. Frunzio, S. Girvin, M. Devoret, and R. Schoelkopf, Nature (London) **467**, 574 (2010).
[8] L. Childress, A. Sørensen, and M. Lukin, Phys. Rev. A **69**, 042302 (2004).
[9] G. Burkard and A. Imamoglu, Phys. Rev. B **74**, 041307 (2006).
[10] M. Trif, V. Golovach, and D. Loss, Phys. Rev. B **77**, 045434 (2008).
[11] G. Guo, H. Zhang, Y. Hu, T. Tu, and G. Guo, Phys. Rev. A **78**, 020302 (2008).
[12] N. Lambert, Y.-N. Chen, R. Johansson, and F. Nori, Phys. Rev. B **80**, 165308 (2009).
[13] A. Cottet and T. Kontos, Phys. Rev. Lett. **105**, 160502 (2010).
[14] A. Cottet, C. Mora, and T. Kontos, Phys. Rev. B **83**, 121311 (2011).
[15] M. Hofheinz *et al.*, Nature (London) **459**, 546 (2009).
[16] H. Wang *et al.*, Phys. Rev. Lett. **106**, 060401 (2011).
[17] A. Houck *et al.*, Nature (London) **449**, 328 (2007).
[18] O. Astafiev, K. Inomata, A. Niskanen, N. Y. Pashkin, Yu. A, and J. Tsai, Nature (London) **449**, 588 (2007).
[19] M. Sandberg, C. Wilson, F. Persson, T. Bauch, G. Johansson, V. Shumeiko, T. Duty, and P. Delsing, Appl. Phys. Lett. **92**, 203501 (2008).
[20] C. M. Wilson, T. Duty, M. Sandberg, F. Persson, V. Shumeiko, and P. Delsing, Phys. Rev. Lett. **105**, 233907 (2010).
[21] T. Niemczyk *et al.*, Nat. Phys. **6**, 772 (2010) .
[22] A. Fedorov, A. K. Feofanov, P. Macha, P. Forn-Diaz, C. J. P. M. Harmans, and J. E. Mooij, Phys. Rev. Lett. **105**, 060503 (2010).
[23] P. Forn-Diaz, J. Lisenfeld, D. Marcos, J. J. Garcia-Ripoll, E. Solano, C. J. P. M. Harmans, and J. E. Mooij, Phys. Rev. Lett. **105**, 237001 (2010).
[24] J. Casanova, G. Romero, I. Lizuain, J. J. Garcia-Ripoll, and E. Solano, Phys. Rev. Lett. **105**, 263603 (2010).
[25] S. Ashhab and F. Nori, Phys. Rev. A **81**, 042311 (2010).
[26] J. Hausinger and M. Grifoni, Phys. Rev. A **82**, 062320 (2010).
[27] J. Basset, H. Bouchiat, and R. Deblock, Phys. Rev. Lett. **105**, 166801 (2010).
[28] Y. A. Pashkin, H. Im, J. Leppäkangas, T. F. Li, O. Astafiev, A. A. Abdumalikov, E. Thuneberg, and J. S. Tsai, Phys. Rev. B **83**, 020502 (2011).
[29] M. Hofheinz, F. Portier, Q. Baudouin, P. Joyez, D. Vion, P. Bertet, P. Roche, and D. Esteve, Phys. Rev. Lett. **106**, 217005 (2011).
[30] M. Marthaler, G. Schön, and A. Shnirman, Phys. Rev. Lett. **101**, 147001 (2008).
[31] T. Frey, P. Leek, M. Beck, K. Ensslin, A. Wallraff, and T. Ihn, Appl. Phys. Lett. **98**, 262105 (2011a).
[32] M. Delbecq, V. Schmitt, F. Parmentier, N. Roch, J. Viennot, G. Fève, B. Huard, C. Mora, A. Cottet, and T. Kontos, Phys. Rev. Lett. **107**, 256804 (2011).
[33] T. Frey, Leek, M. P. J. Beck, A. Blais, T. Ihn, K. Ensslin, and A. Wallraff, e-print arXiv:1108.5378 (unpublishedb).
[34] P.-Q. Jin, M. Marthaler, J. H. Cole, A. Shnirman, and G. Schön, Phys. Rev. B **84**, 035322 (2011).
[35] D. A. Rodrigues, J. Imbers, and A. D. Armour, Phys. Rev. Lett. **98**, 067204 (2007).
[36] G. Ingold and Y. Nazarov, in *Single Charge Tunneling*, edited by M.H. Devoret and H. Grabert, NATO ASI Series B (Plenum Press, New York, 1992), Vol. 294, p. 21.
[37] P. Delsing, K. K. Likharev, L. S. Kuzmin, and T. Claeson, Phys. Rev. Lett. **63**, 1180 (1989).

[38]S. M. Girvin, L. I. Glazman, M. Jonson, D. R. Penn, and M. D. Stiles, Phys. Rev. Lett. **64**, 3183 (1990).
[39]M. H. Devoret, D. Esteve, H. Grabert, G. Ingold, H. Pothier, and C. Urbina, Phys. Rev. Lett. **64**, 1824 (1990).
[40]A. N. Cleland, J. M. Schmidt, and J. Clarke, Phys. Rev. Lett. **64**, 1565 (1990).
[41]T. Holst, D. Esteve, C. Urbina, and M. H. Devoret, Phys. Rev. Lett. **73**, 3455 (1994).
[42]H. Park, J. Park, A. Lim, E. Anderson, A. Alivisatos, and P. McEuen, Nature (London) **407**, 57 (2000).
[43]D. Boese and H. Schoeller, Europhys. Lett. **54**, 668 (2001).
[44]S. Braig and K. Flensberg, Phys. Rev. B **68**, 205324 (2003).
[45]A. Mitra, I. Aleiner, and A. J. Millis, Phys. Rev. B **69**, 245302 (2004).
[46]S. Sapmaz, P. Jarillo-Herrero, Y. Blanter, C. Dekker, and H. Van der Zant, Phys. Rev. Lett. **96**, 026801 (2006).
[47]R. Leturcq, C. Stampfer, K. Inderbitzin, L. Durrer, C. Hierold, E. Mariani, M. Schultz, F. Von Oppen, and K. Ensslin, Nat. Phys. **5**, 327 (2009).
[48]J. Koch and F. von Oppen, Phys. Rev. Lett. **94**, 206804 (2005a).
[49]F. Haupt, F. Cavaliere, R. Fazio, and M. Sassetti, Phys. Rev. B **74**, 205328 (2006).
[50]J. Koch and F. von Oppen, Phys. Rev. B **72**, 113308 (2005b).
[51]J. Koch, F. von Oppen, and A. V. Andreev, Phys. Rev. B **74**, 205438 (2006).
[52]X. Y. Shen, B. Dong, X. L. Lei, and N. J. M. Horing, Phys. Rev. B **76**, 115308 (2007).
[53]M. Merlo, F. Haupt, F. Cavaliere, and M. Sassetti, New J. Phys. **10**, 023008 (2008).
[54]Z. Ioffe, T. Shamai, A. Ophir, G. Noy, I. Yutsis, K. Kfir, O. Cheshnovsky, and Y. Selzer, Nat. Nanotechnology **3**, 727 (2008).
[55]R. Hartle and M. Thoss, Phys. Rev. B **83**, 125419 (2011).
[56]G. Piovano, F. Cavaliere, E. Paladino, and M. Sassetti, Phys. Rev. B **83**, 245311 (2011).
[57]M. Castellanos-Beltran and K. Lehnert, Appl. Phys. Lett. **91**, 083509 (2007).
[58]M. Castellanos-Beltran, K. Irwin, G. Hilton, L. Vale, and K. Lehnert, Nat. Phys. **4**, 929 (2008).
[59]B. Yurke and J. S. Denker, Phys. Rev. A **29**, 1419 (1984).
[60]M. H. Devoret, in *Quantum Fluctuations*, edited by S. Reynaud, E. Giacobino, and J. Zinn-Justin (Elsevier, Amsterdam, 1997).
[61]E. Paladino, F. Taddei, G. Giaquinta, and G. Falci, Physica E **18**, 39 (2003).
[62]J. Koch, A. A. Houck, K. L. Hur, and S. M. Girvin, Phys. Rev. A **82**, 043811 (2010).
[63]H. Goldstein, C. Poole, J. Safko, and S. Addison, *Classical Mechanics* (Addison-Wesley, 2002).
[64]U. Weiss, *Quantum Dissipative Systems* (World Scientific, 2008).
[65]G. Mahan, *Many-particle Physics* (Plenum, 2000).
[66]For models in molecular electronics higher order, anharmonic terms in the phonon modes effectively make the charging energy positive for sufficiently many electrons on the dot for arbitrary strong electron-phonon coupling. Such anharmonic terms are not present in our system where the exact Hamiltonian is quadratic in all variables.
[67]C. Gardiner and P. Zoller, *Quantum Noise* (Springer Verlag, 2004).
[68]D. A. Rodrigues and A. D. Armour, New J. Phys. **7**, 251 (2005).
[69]H. Hübener and T. Brandes, Phys. Rev. B **80**, 155437 (2009).
[70]M. Wallquist, V. S. Shumeiko, and G. Wendin, Phys. Rev. B **74**, 224506 (2006).
[71]A. Donarini, A. Yar, and M. Grifoni, e-print arXiv:1109.0723 (unpublished).
[72]N. Traverso Ziani, G. Piovano, F. Cavaliere, and M. Sassetti, Phys. Rev. B **84**, 155423 (2011).
[73]M. Devoret, S. Girvin, and R. Schoelkopf, Ann. Phys. **16**, 767 (2007).
[74]D. Bozyigit *et al.*, Nat. Phys.**7**, 154 (2010).
[75]C. Eichler, D. Bozyigit, C. Lang, L. Steffen, J. Fink, and A. Wallraff, Phys. Rev. Lett. **106**, 220503 (2011).
[76]C. Eichler, D. Bozyigit, C. Lang, M. Baur, L. Steffen, J. M. Fink, S. Filipp, and A. Wallraff, Phys. Rev. Lett. **107**, 113601 (2011).
[77]M. Hofheinz, E. Weig, M. Ansmann, R. Bialczak, E. Lucero, M. Neeley, A. O'Connell, H. Wang, J. Martinis, and A. Cleland, Nature (London) **454**, 310 (2008).
[78]K. E. Cahill and R. J. Glauber, Phys. Rev. **177**, 1882 (1969).
[79]R. Hartle and M. Thoss, Phys. Rev. B **83**, 115414 (2011).
[80]D. F. Urban, R. Avriller, and A. Levy Yeyati, Phys. Rev. B **82**, 121414 (2010).
[81]T. Novotný, F. Haupt, and W. Belzig, Phys. Rev. B **84**, 113107 (2011).
[82]F. Haupt, T. Novotný, and W. Belzig, Phys. Rev. Lett. **103**, 136601 (2009).
[83]T. Frederiksen, M. Paulsson, M. Brandbyge, and A.-P. Jauho, Phys. Rev. B **75**, 205413 (2007).
[84]Y. Blanter and M. Büttiker, Phys. Rep. **336**, 1 (2000).
[85]S. Kafanov and P. Delsing, Phys. Rev. B **80**, 155320 (2009).
[86]D. A. Bagrets and Y. V. Nazarov, Phys. Rev. B **67**, 085316 (2003).
[87]C. Flindt, T. Novotný, and A. Jauho, Europhys. Lett. **69**, 475 (2005).
[88]G. Kießlich, P. Samuelsson, A. Wacker, and E. Schöll, Phys. Rev. B **73**, 033312 (2006).
[89]A. Braggio, J. König, and R. Fazio, Phys. Rev. Lett. **96**, 026805 (2006).
[90]A. Yar, A. Donarini, S. Koller, and M. Grifoni, Phys. Rev. B **84**, 115432 (2011).
[91]C. Flindt, T. Novotný, and A. P. Jauho, Phys. Rev. B **70**, 205334 (2004).